HHS Public Access

Author manuscript

Chem Soc Rev. Author manuscript; available in PMC 2019 May 21.

Published in final edited form as:

Chem Soc Rev. 2018 May 21; 47(10): 3621–3639. doi:10.1039/c8cs00080h.

Catalytic Peptide Assemblies

O. Zozulia, M.A.[†], **Dolan**[†], and **IV Korendovych**

Department of Chemistry, Syracuse University, 111 College Place, Syracuse NY, 13244, USA

Abstract

Self-assembly of molecules often results in new emerging properties. Even very short peptides can self-assemble into structures with a variety of physical and structural characteristrics. Remarkably, many peptide assemblies show high catalytic activity in model reactions reaching efficiencies comparable to those found in natural enzymes by weight. In this review, we discuss different strategies used to rationally develop self-assembled peptide catalysts with natural and unnatural backbones as well as with metal-containing cofactors.

Graphical abstract

Peptides can self-assemble to form catalytic aggregates with activities comparable to those of natural enzymes.

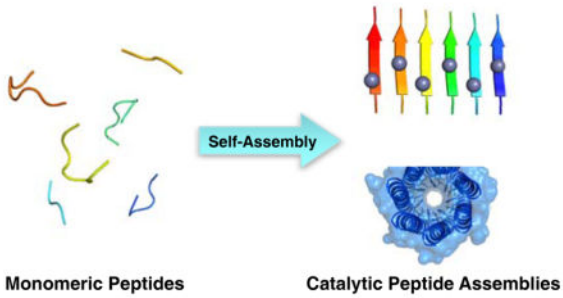

1. Introduction

While the thermodynamic difficulties in promoting chemical reactions, i.e. where to get energy for a particular chemical transformation, can appear quite formidable, the real challenge lays in channeling this energy into a particular direction. The Earth receives more than enough energy from the Sun to sustain any human demands.[1] Moreover, nature has evolved tools to harvest light to ultimately convert its energy into making and breaking chemical bonds with extraordinary efficiency and selectivity. At the same time, the ever-expanding demand for new commodities, pharmaceuticals and materials drives discovery of new catalysts for reactions nature has not deemed necessary for life.

[†]These authors contributed equally.

Conflicts of interest

There are no conflicts to declare.

Incredible catalytic efficiency as well as regio- and stereospecificity exhibited by enzymes is truly remarkable, as few industrial catalysts can match their performance.[2] On the other hand, such efficiency comes at a price – many enzymes are large polypeptides that can be difficult and expensive to produce and utilize. Intuitively, it seems that complex enzymes must have evolved from much less complex molecules after many iterations in a bottom-up approach. Amino acids, one of many key ingredients of the "primordial soup",[3] can be produced from inorganic compounds.[4] These basic building blocks of proteins have been hypothesized to condense into larger peptides[5–8] potentially proceeding via an "amyloid world".[9–11] As even very short peptides can catalyze quite a variety of chemical transformations[12–14] it seems quite logical that their subsequent improvement can yield incredibly efficient enzymes. While many gaps remain in our understanding of prebiotic chemistry (and it is entirely possible that we will never be able to truly deduce enzymes' origins with certainty), it is plausible that assembly of small building blocks into larger, more complex structures has played a significant role on early Earth.

Self-assembly of molecules has long been known to result in new emerging properties and the rapid rise and prominence of nanotechnology is a testament to its major practical and fundamental significance.[15] Peptides provide many routes for self-assembly due to the interplay between van der Waals forces, hydrogen bonding, electrostatic, and stacking interactions[16] to allow for formation of various supramolecular structures driven by subtle changes in hydrophobicity, charge, and size of the peptides. As a result, peptides can form coil-coiled bundles,[17–20] amphiphilic amyloid peptides,[21–23] hydrogels[24–26] as well as other motifs[27–29] in a controlled manner. Synthetic modifications beyond the naturally available amino acids (e.g. installing alkyl tails, or aromatic groups capable of π-stacking) provide additional opportunities to create a large variety of supramolecular architectures including sheets, twisted or linear fibers, spheres, tapes, and tubes.[30]

Despite the obvious appeal, creating efficient catalysts through self-assembly of peptides is far from easy. Indeed, the very same factors that favor the existence of self-assembled peptide catalysts can be detrimental to their rapid development. Developing meaningful structure-activity relationships can be difficult given the hyperastronomical sequence spaces possible even with small sequences, especially in the absence of accurate modeling tools. Moreover, the incredible diversity of possible tertiary and quaternary structures can be difficult to characterize using traditional "small molecule" tools. Thus, at the moment the interface of the fields of catalysis, self-assembly and peptides appears to be quite limited (Figure 1).

On the bright side, development of computational tools (e.g. Rosetta) for protein design together with advances in electron microscopy and nuclear magnetic resonance (NMR) allowed for a rapid growth of the field that has been covered previously in some or all aspects in several excellent reviews.[31–35] In this paper, we will discuss recent progress in developing self-assembling peptide catalysts with and without additional cofactors.

2. Self-assembled peptide catalysts forming distinct oligomers

Understanding of the basic principles of peptide self-assembly in the 1970s and the 1980s drove the first attempts to produce catalysts. The application of the concept of self-assembly to catalyst design was particularly appealing since relatively large assemblies can be predictably modeled and put together using small building blocks that are easy to produce and characterize. In the earliest example of this approach Benner and co-workers[36] rationally designed a 14-mer alpha-helical peptide that formed helical bundles capable of catalyzing decarboxylation of oxaloacetate to pyruvate. The rate of formation of the imine by the artificial catalyst is three to four orders of magnitude faster than that of an amine molecule.

The use of four-helix bundles to catalyze various chemical reactions was pioneered by Baltzer *et al.* who designed KO-42, a 42-residue polypeptide that folded into a helix-loop-helix hairpin motif. KO-42 dimerizes into an antiparallel four-helix bundle as shown by NMR, circular dichroism (CD) spectroscopy and ultracentrifugation and catalyzes hydrolysis of *p*-nitrophenyl esters (Fig. 2).[37] The catalysis is promoted by histidine residues engineered on the surface of the folded polypeptide. The reaction follows second-order kinetics in water or water-trifluoroethanol mixtures, with rate constants that are 10^3 times larger than those shown by 4-methyl imidazole and five orders of magnitude above the rate of the non-catalyzed reaction.

Subsequent attempts to better understand the mechanism of KO-42's catalysis resulted in development of modified variants JN-42, MN-42 as well as MKNR. These peptides contained either fewer histidine residues or additional arginine, lysine or glutamine moieties to stabilize the transition state. While the modified variants showed lower efficiency for *p*-nitrophenyl ester hydrolysis, they showed chiral substrate recognition: *p*-nitrophenyl ester of D-norleucine was hydrolyzed faster than its L-enantiomer.[38] Subsequent sequence optimization and kinetic studies highlighted the importance of the pK_a of the active histidine as well as the geometry of the active site in catalyzing ester hydrolysis.[39, 40]

The helical bundles formed by the helix-loop-helix motif can be used for hydrolysis of more challenging substrates such as phosphodiesters.[41] The active site was constructed to include two histidine and four arginine residues, with the capacity to provide general acid, general base, and/or nucleophilic catalysis as well as transition state stabilization. The resulting peptide catalyst catalyzed hydrolysis of uridine 3′-2,2,2-trichloroethylphosphate, a mimic of RNA, with a second order rate constant of 2.5×10^{-2} M^{-1} min^{-1}, an increase of 300-fold over the imidazole-catalyzed reaction. Further improvement of the catalytic activity was achieved by introducing tyrosine residues close to the active site.[42]

Baltzer and co-workers expanded their approach in creating self-assembling catalysts to other types of reactions as well. Aldimine binding sites were introduced into the peptides of the KO-42 family to catalyze conversion of aldimine into ketamine, emulating the biosynthesis of amino acids. The design process employed incorporation of His residues capable of facilitating the rate-limiting 1,3-proton transfer step of the transamination reaction. Introduction of charged residues to stabilize negatively charged substituents on the

aldimine was another important feature of the design. The resulting catalysts T-4 and T-16 bound the aldimines with mM affinity and catalyzed conversion of aldimine into ketamine with the rates that are more than three orders of magnitude faster than that of imidazole (Fig. 2, bottom).[43]

Self-assembly of carefully engineered subunits can result in formation of highly complex and versatile catalysts. Matille and co-workers designed octiphenyl-based rigid-rod staves[44, 45] to which leucine-histidine pentapeptides with the sequence of LHLHL were covalently attached (Fig. 3). The monomers self-assemble into supramolecular β-barrel esterases with hydrophobic exterior and histidine-rich pore interior of the catalytic pores.[46, 47] The catalytic activity of these supramolecular assemblies extends to RNA hydrolysis,[48] amide and carbonate hydrolysis as well as cofactor-promoted chemospecific but not enantioselective esterolysis.[49] The catalytic pores can be embedded in phospholipid vesicles forming highly stable, multifunctional ion channels.[50]

Efficient catalysis promoted by supramolecular assemblies does not require large macromolecules. Tagging of proline with an amido naphthyridine (Nap) by Clarke and co-workers yielded Pro-Nap, a minimal peptide that can hydrogen bond to a variety of organic molecule co-catalysts providing a library of asymmetric assemblies capable of enamine catalysis (Scheme 1).[51] Good yields, good to excellent diastereomeric ratios (*dr*), in some cases good enantioselectivity was achieved using these catalysts in nitro-Michael reaction with various substrates.

From a single functional group to concerted action of multiple functional groups

The catalysts described above employed a very simple approach to achieving catalysis: a single functional group is placed in a self-assembling scaffold to achieve substrate binding; additional secondary interactions are then introduced and optimized in an effort to further improve the reactivity. Considering that natural proteins rely on *precise* three-dimensional arrangement of functional groups, it is not surprising that the resulting activity of *de novo* designed catalysts is inferior to that of the enzymes. While much is known about the concerted action of multiple residues in enzymes, replicating such arrangements is very difficult.[52] Woolfson and co-workers developed an artificial esterase based on homo-heptameric assembly of *de novo* designed helices.[53] The toroid topology of the self-assembled catalyst should facilitate substrate binding and turnover (Fig. 4).

A catalytic triad consisting of a glutamate, a histidine and a cysteine was introduced into each α-helix to face the hydrophobic interior of the assembly as confirmed by X-ray crystallography. The resulting assembly hydrolyzes para-nitrophenyl acetate (*p*-NPA) in a two-step, enzyme-like multi-turnover process, where fast acylation of the active nucleophile is followed by a rate-limiting hydrolysis, with an overall enzymatic efficiency that is comparable to those of other reported designed esterases.[54]

Catalytic assemblies with metal cofactors

The use of metallocofactors to facilitate catalysis in coiled coils was pioneered by DeGrado. Metals facilitate various chemical transformations and promote self-assembly at the same time. Homomeric peptide assemblies greatly simplify the development of catalysts since

only one polypeptide chain needs to be designed. Despite the seeming simplicity, very complicated structures that provide well-defined primary and secondary coordination spheres can be obtained by this approach. Incorporation of the secondary interactions is crucial as polar metal-coordinating residues must be properly positioned not just to bind the metal ions but to keep the hydrophobic core of the bundle from falling apart.

Kaplan and DeGrado developed a heterotetrameric coiled-coil DFtet comprised of two different "A" and "B" subunits from the first principles.[55] When mixed together in the appropriate stoichiometry the peptides self-assemble to form an asymmetric helical bundle that binds two iron(II) ions in its active site. The resulting assembly catalyzes two-electron oxidation of 4-aminophenol to the corresponding quinone monoimine by dioxygen. The high catalytic efficiency (k_{cat}/K_M = 1,500 M^{-1} min^{-1}) and substrate recognition of DFtet can be further tuned, illustrating the specificity of the design.[56] Based on the lessons learned from DFtet, the DeGrado lab developed a single chain version of the bundle (DFsc) that promotes a wide range of chemical transformations (Fig. 5).[57, 58]

Pecoraro and coworkers have greatly advanced the understanding of the basic principles that drive self-assembly of helices into catalytic three-helix bundles. The 3-fold symmetry of the bundle is well suited for binding metal ions that prefer lower coordination numbers. Incorporation of cysteine residues into the hydrophobic region of the bundle allowed for creation of well-folded, highly stable (K_{assoc}> 10^7 M^{-1}) peptide-metal complexes of cadmium, lead and mercury. Modification of the primary sequences of the resulting parallel bundles offers additional fine-tuning of metal ion properties and enables incorporation of multiple metal-binding sites.[59–61]

Taken together, the stability of the bundle provided by tight association of thiolates with mercury and ability to provide multiple metal binding sites allowed for creation of an artificial metallohydrolase (Fig. 6, top). The *de novo* designed enzyme $[Hg(II)]_S[Zn(II)(OH^-)]_N(TRIL9CL23H)_3$ utilized a histidine-bound zinc cofactor to hydrolyze *p*-NPA and to catalyze CO_2 hydration. Its catalytic efficiency of 1398 ± 18 M^{-1} min^{-1} in *p*-NPA hydrolysis compared favorably to previously reported artificial hydrolases and is only two orders of magnitude lower than that of carbonic anhydrase. The ability of $[Hg(II)]_S[Zn(II)(OH^-)]_N(TRIL9CL23H)_3$ to facilitate CO_2 hydration reaction is also quite remarkable: the catalytic efficiency reaches 1.08 ± 0.18 x 10^7 M^{-1} min^{-1} at pH 9.5. This rate is over 70-fold faster than that of any previously reported model and within 500-fold of carbonic anhydrase.[62] The structure of the metallohydrolase solved by X-ray crystallography confirmed the design (Fig. 6, bottom).

Subsequent systematic optimization of $[Hg(II)]_S[Zn(II)(OH^-)]_N(TRIL9CL23H)_3$ showed that while the active site location for the catalytic His_3O-Zn(II) site influences the maximal rate, substrate access, and metal binding affinity, the catalytic activity is preserved in all cases.[63] This finding allowed Pecoraro and co-workers to move beyond the original parallel helix arrangement by utilizing a_3D protein, an anti-parallel 73-residue 3-helical bundle protein developed in the DeGrado lab.[64] Three of the core leucine residues of a_3D were mutated to histidines to create a new active site capable of *p*-NPA hydrolysis and CO_2 hydration (Fig. 7).[65] The resulting metalloenzyme Zn(II)α_3DH3 shows somewhat lower

activity compared to that of $[Hg(II)]_S[Zn(II)(OH^-)]_N(TRIL9CL23H)_3$, however it is likely to have higher evolvability potential due to its single polypeptide chain.

The simple coordination spheres of *de novo* designed trimeric coiled coils can accommodate metals other than zinc. Copper provides access to redox chemistry, but development of efficient redox catalysts can be challenging due to the necessity of tight binding of the active site metal ion in all oxidation states along the catalytic cycle. Pecoraro and co-workers showed that copper-binding trimeric coiled coils satisfy this stringest requirement by designing $Cu(I/II)(TRIL23H)_3$, a functional model for the Cu_{T2} center of copper nitrite reductase (Fig. 8).[66]

Upon self-assembly the copper ion binds three histidine residues of TRIL23H, a close relative of TRIL9CL23H that has cysteines reverted back to leucine residues, leaving two sites open to substrate/reductant coordination. The active site in the model enzyme was experimentally found to be similar to that of the Cu_{T2} center; with nM-μM affinity for the Cu(II) and pM affinity for the Cu(I). At the optimal pH of 5.8, $Cu(II)(TRIL23H)_3$ catalyzes reduction of nitrate to nitric oxide by ascorbate for at least five turnovers with no loss of catalytic efficiency after 3.7 h. While activity of $Cu(II)(TRIL23H)_3$ is still about six orders of magnitude less that that found in the natural enzymes[67] this *de novo* designed water-soluble homogeneous catalyst can likely be substantially further evolved by directed evolution.

Coiled coils can also accommodate complex metal-containing cofactors. Metalloporphyrins offer incredible functional versatility as well as additional possibilities for non-covalent interactions with the peptide bundle. The basic principles that drive assembly of helical bundles has been well established both for soluble[68] and membrane[69] peptides.

Ghirlanda and co-workers have reported the first example of self-assembling membrane peroxidase ME1 that takes advantage of dimerization of a eukaryotic protein glycophorin A (GpA). Introducing a histidine residue into the peptide derived from the transmembrane domain of GpA created a binding site with sub-micromolar affinity for hemin. The ME1–heme complex (Fig. 9, left) solubilized by dodecyl phosphatidylcholine (DPC) promotes oxidation of 3,3′,5,5′-tetramethylbenzidine (TMB) by hydrogen peroxide (H_2O_2) in two successive one-electron processes with the rate 2-fold above the background.

Mahajan and Bhattacharjya demonstrated that rationally designed β-hairpin peptides can functionally bind hemin in the membrane environment to provide peroxidase activity.[70] The peptides, termed IV8 and IV8FA, were designed to contain a membrane anchoring myristoyl (Myr) group, a ^{D}Pro-Gly segment for the nucleation of a type I′ or type II′ β-turn and a heme binding histidine residue (Fig. 9, right). Additionally, a Trp residue was introduced to interact with the groups at the water-lipid interface. The peptides bind heme in DPC micelles with 2:1 stoichiometry and the resulting assemblies catalyze oxidation of TMB by H_2O_2 with activity comparable to that of ME1 despite its much smaller size. Neither the heme nor peptide independently showed any detectable peroxidase activity.

Of note is the work of Anderson *et al.* who have designed an artificial heme-dependent peroxidase C45.[71] This peptide, while not a self-assembling bundle itself, is based on the

previously reported tetrameric parallel coiled-coil developed by Dutton.[72] C45 showed very high activity in oxidizing model substrates surpassing those of some naturally occurring peroxidases. This artificial enzyme is extremely robust, thermostable and tolerant of organic solvents (Fig. 10).

The repertoire of metals that can be employed in self-assembling peptide catalysts is quite versatile. Laungani and co-workers[73] developed complementary C- and *N*-terminal phosphane-functionalized peptides to bind noble metals (Pt/Rh) (Fig. 11). Upon mixing, the peptides and appropriate metal salts form β-sheet assemblies that can do asymmetric hydroformylation of styrene with quantitative yield and excellent (in some cases as high as 95:5) regioselectivity but modest (up to only 38% ee) enantioselectivity.

Design of metal sites on protein interfaces

Catalytic sites can be computationally engineered at the interfaces of existing peptides and proteins to drive assembly. In attempt to design a zinc-mediated protein-protein interface Kuhlman and co-workers[74] discovered that the resulting assembly MID1 was capable of catalyzing ester and phosphoester hydrolysis. MID1-zinc hydrolyzes *p*-NPA with a k_{cat}/K_M of 3.78 x 10^4 M^{-1} min^{-1}, and *p*-nitrophenyl phosphate (*p*-NPP) with a k_{cat}/K_M of 840 M^{-1} min^{-1}, a quite remarkable acceleration for a serendipitously found, unoptimized catalyst. X-ray structural studies revealed three-coordinated catalytic zinc located at a homodimer interface cleft (Fig. 12).

Song and Tezcan reported an artificial hydrolase Zn_8:$AB3_4$ constructed by designing zinc binding sites on a monomeric redox protein cyt bc_{562} (Fig. 13A).[75] Upon addition of zinc Zn_8:$AB3_4$ tetramerizes with eight metal ions bound (Fig. 13B, C) and promotes hydrolysis of *p*-nitrophenol esters, nitrocephin and ampicillin. *E. coli* expressing the catalyst in the periplasm showed survival on antibiotic plates with low concentration of ampicillin. Subsequent optimization of the catalyst using rational design and directed evolution led to limited improvement in catalytic efficiency.[76]

Peptides with unnatural backbones

Lessons learned from working with α-peptides can be extended to polypeptide structures formed by unnatural amino acids. β-peptides, formed by β-amino acids that have three carbons in the main chain with a branching point in position 3 (next to the amino group, Fig. 14A), are arguably the most characterized group of these foldamers.[77, 78] Recent advances in computational modelling allowed for creation of well-defined self-assembled 3_{14}-helical bundles in various oligomeric states[79–82] and even mixed α-peptide/β-peptide assemblies.[83] In terms of catalysis, however, there are only two examples of catalytic assemblies emerging from self-assembly of β-peptides.

Gellman, Hilvert and co-workers[84] used conformationally rigid ACHC (trans-2-aminocyclohexanecarboxylic acid)-based scaffold with heptanoyl tails to create a highly robust dimeric structure (Fig. 14A). Incorporation of β-Lys residues into the β-peptide conferred ability to catalyze retroaldol reaction onto the foldamer. The foldamer's activity in a model cleavage of β-hydroxyketone can be described by a Michaelis-Menten formalism with kinetic parameters of k_{cat} and K_M of 0.13 ± 0.01 min^{-1} and 5.0 ± 0.6 mM, respectively.

This level of activity compares well to the state-of-the-art computationally designed retroaldolase.[85]

Schepartz and co-workers designed a series of β^3-peptide octameric bundles capable of both substrate binding and ester hydrolysis. The best catalyst βEst-28-2R (3rd generation catalyst design) promoted hydrolysis of 8-acetoxypyrene-1,3,6-trisulfonate to form fluorescent pyranine (Fig. 14B) with catalytic efficiency of 6446 M^{-1} min^{-1} and a k_{cat}/k_{uncat} value of 820. Importantly, the activity was shown to originate from concerted action of multiple residues located on different strands that comprise the octameric bundle.[86]

3. Self-assembled peptide catalysts forming large oligomers

Proline-based catalysts

The incredible progress documented in the previous chapter suggests great promise for the emerging catalytic properties of self-assembled peptides. Distinct low order oligomers with catalytic properties can be relatively easily structurally characterized providing mechanistic insight and spurring subsequent optimization. At the same time, the very nature of these oligomers imposes quite a few restrictions on the design process. For example, in coiled-coils too many charged residues in the hydrophobic core of the bundle can lead to unfolding and additional stabilization is then required, which can take a lot of time and effort. Moreover, while in principle all three positions per heptad not involved in assembly can be used to introduce catalytic residues, only the residue facing the interior of the bundle is typically employed.

Alternatively, one can envision self-assembly driven without regard to formation of a predetermined molecular structure. In the simplest case a residue with a functional group can be linked to a peptide fragment that strongly promotes self-assembly and the resulting supramolecular structure gains improved activity, efficiency, selectivity, etc. (Scheme 2).

Proline is arguably the most versatile single amino acid residue from the 20 translationally incorporated ones. It has been extensively (and successfully!) used for catalysis,[87–96] thus it is not surprising that it was in the focus of early work on self-assembled peptides.

Miravet, Escuder and co-workers covalently linked a Pro-Val dipeptide with various alkyl fragments to induce gelation and to promote enamine based catalysis (Fig. 15). Efficient and stereoselective conversion of substrates was only observed if the peptide catalyst self-assembled into long fibrils and required an aliphatic tail of at least 12 carbon atoms in the case of a single chain or 8 atoms when connecting two dipeptide moieties (**14** and **15**, Fig. 15).[97,98] Rheologically, the self-assembled peptides behave as hydrogels: the representative G' and G'' values for **15** in nitromethane at 10 mM were equal to 100 and 1000 Pa respectively, whereas at 20 mM the same compound demonstrated a 10^4 increase in G' and G'' values. The effects of increasing temperature, aging time, ultrasound, and change of pH on morphology have been extensively studied. Depending on the preparation conditions, the hydrogel catalyst **14** was found to have three different characterized polymorphic structures, however all of them converted substrate to the aldol product with similar yields, stereo- and

enantioselectivity after 24 hours. Moreover, catalytic hydrogels can be reused without major losses in the activity or selectivity.

The proline-based self-assembled peptide hydrogels have also been used to catalyze direct aldol reaction,[99–101] 1,4-conjugated addition of ketones to alkenes,[102] and the Mannich reaction.[103] While the early examples of reactions catalyzed by these assemblies showed no diastereoselectivity and enantioselectivity,[99] quantitative yield with 92:8 *anti/syn* ratio and 90% enantiomeric excess (*ee*) was observed in some cases.[101, 102, 104]

Supramolecular proline-based peptide assemblies have been successfully applied to more complex transformations such as one-pot deacetalization–aldol tandem reactions (Scheme 3) and asymmetric Mannich reaction (Scheme 4, reaction [**7**]).[103, 105] Interestingly, when mixtures of peptide catalysts were used to catalyze tandem reactions the best diastereoselective conversion (up to 91% yield, *anti/syn* ratio of 90:10 and 91% *ee*) of the starting material was achieved only when the catalyst was comprised of self-sorted fibrils and not co-assembled ones (Scheme 3). This effect was explained by deactivation of the reactive sites in co-assembled fibrils. When the same system was used in Mannich reaction excellent yields and diastereoselectivity was observed (94% yield, *anti/syn* ratio of 95:5 and 60% *ee*).

The approach of attaching long hydrophobic tails to proline-containing peptides is quite permissive in respect to the primary sequence of the catalyst. A Pro-Arg-Trp tripeptide with C-terminal palmitoyl tail (PRW-C_{16}) was shown to self-assemble into spherical micelles that catalyzed aldol reaction between cyclohexanone and *p*-nitrobenzaldehyde in water. Under optimized conditions quantitative yield, high diastereoselectivity (92:8) and good enantioselectivity (up to 85% *ee*) were reported.[106] Liu and co-workers observed that amphiphilic peptide Pro-Trp with alkyl chains on amidated C-terminus catalyzes asymmetric aldol reaction of cyclohexanone with *p*-nitrobenzaldehyde in water.[108] The enantioselectivity of the reaction is dependent on morphology of the assembly - the nanospheres provide higher selectivity than nanofibers. Compressed carbon dioxide allows for regulation of peptide self-assembly leading to excellent dia- and enantioselectivity in some cases.[109]

Self-assembly can be also achieved via attachment of various peptide sequences known to drive aggregation. $P(FE)_n$ or $P(EF)_n$ peptides with long alkyl chains at C-termini easily form hydrogels that catalyze direct aldol reaction dia- and enantioselectively (Fig. 16).[107] The hydrogels showed good stereoselectivity in promoting self-condensation of α-oxy-aldehydes and phenylalkyl aldehydes. Interestingly, the reaction kinetics cannot be described by the typical Michaelis–Menten in this case. Mechanistic studies performed on this system suggest that the presence of hydrophobic regions aids substrate solubilization, and the active site accessibility is the key factor for the observed differences in reaction rates.

Parquette and co-workers attached 1,4,5,8-naphthalenetetracarboxylic acid diimide (NDI) to a proline-lysine dipeptide. The resulting molecule assembled into catalytic nanotubes formed by bilayers of peptides, where proline residues are accessible along both the inner and outer surface of the assembly (Fig. 17).[110] The nanotubes show moderate to good yields,

diastereoselectivity and in some cases even good enantioselectivity in aldol reactions with nitroaldehydes. Importantly, these catalytic assemblies are reusable following a cycle of ultracentrifugation-resuspension.

Histidine-based self-assembled peptides

Much attention has been given to development of self-assembling catalysts for hydrolytic reactions due to their practical importance and the ease of measurement. While a single amino acid histidine on its own is capable of promoting hydrolysis, the catalytic efficiency is very low. However, incorporation of histidine into self-assembling structures has emerged as a powerful strategy for creating artificial hydrolases.

Guler and Stupp installed two histidine residues into self-assembling peptide amphiphiles that contain a short peptidic sequence with an alkyl chain covalently attached to the N-terminus. The resulting nanofibrils hydrolyze activated substrates such as 2,4-dinitrophenyl acetate.[111] Importantly, non-fibrillated structures showed poor catalytic activity for the same reaction.

The lessons learned by Escuder, Miravet and Ulijn in creating proline-based self-assembled catalysts described in the previous chapter were applied to the development of fibril esterases. Replacing imidazole with proline in the Pro-Val moiety allowed for moderate hydrolytic activity towards *p*-NPA and non-activated aminoacyl esters (**16**, Fig. 15).[112] Dejugnat and co-workers designed a series of tripeptides containing lypophilic fragments on either termini[113] which catalyzed hydrolysis of *p*-NPA upon self-assembly (Fig. 18A).

Liu and coworkers fused histidine to an Fmoc-FF motif that strongly drives aggregation and demonstrated that Fmoc-FFH-$CONH_2$ self-assembles into catalytic nanotubes capable of facilitating *p*-NPA hydrolysis with the rate of *ca.* 500-fold above the background.[114] These fibrils can be used directly for catalysis or as hybrid capsules with glutaraldehyde crosslinked cationic polyethyleimine.[115] Addition of Fmoc-FFR-$CONH_2$ to Fmoc-FFH-$CONH_2$ results in additional improvement of catalytic activity in a synergistic fashion presumably due to stabilization of the transition state by the guanidyl group of the arginine residue. The dependence of the initial rate on substrate concentration can be fit to a Michaelis-Menten model with k_{cat} and K_M of 8.28 x 10^{-2} min^{-1} and 0.76 mM, respectively, at 1:20 ratio of Fmoc-FFR-$CONH_2$ to Fmoc-FFH-$CONH_2$.

He and co-workers took this approach further and mixed Fmoc-FFH-$CONH_2$ with Fmoc-FFS-$CONH_2$ and Fmoc-FFD-$CONH_2$ at various ratios in an attempt to create an artificial hydrolase with the catalytic Ser/His/Asp triad upon peptide self-assembly into nanofibers (Fig. 18B).[116] Synergistic increase of activity in *p*-NPA hydrolysis was observed upon peptide mixing and substrate imprinting. At the optimal ratio of 40:1:1 (Fmoc-FFH-$CONH_2$ to Fmoc-FFS-$CONH_2$ to Fmoc-FFD-$CONH_2$) catalytic efficiency reached 11.16 M^{-1} min^{-1}, a ~2-fold improvement over the activity of the fibrils formed by Fmoc-FFH-$CONH_2$.

Guler and co-workers used a similar approach to create catalytic triads for hydrolysis of *p*-NPA and acetylthiocholine using peptide amphiphiles.[117] Mixing of peptides with C-terminal serine, histidine and aspartate residues produced peptide nanostructures capable of

efficient catalysis. Assemblies formed by combining all three peptides showed the highest activity followed by dual systems suggesting synergistic interactions between multiple residues.

The Fmoc group or lypophilic tails are not absolutely necessary to promote self-assembly but may enhance the propensity for peptide to self-assemble. Garcia and co-workers reported formation of a thermoreversible hydrogel by $^{L}H^{D}F^{D}F$.[118] Notably, this peptide which does not have any capping groups and contains D-amino acid residues self-assembles and catalyzes *p*-NPA hydrolysis at concentrations of 10 mM and higher. Following similar strategy, longer peptides Q11H (H_2N-HSGQQKFQFQFEQQ-$CONH_2$) and Q11R (H_2N-RSGQQKFQFQFEQQ-$CONH_2$) were co-assembled together at a 10:1 ratio to produce nanofibers (Fig. 19) capable of *p*-NPA hydrolysis.[119]

Using even more complex motifs for aggregation allows for development of extra functionalities. Ulijn and coworkers[120] created a switchable hydrolase by introducing a *N*-terminal histidine in the β-hairpin peptide MAX1 developed by Schneider (Fig. 20).[121–123] The resulting gel-forming peptide VK2H is pH-responsive just like the parent compound and upon formation of a hydrogel catalyzes hydrolysis of *p*-NPA with catalytic efficiency of 1151 M^{-1} min^{-1}.

Biocompatibility of peptides allows for utilizing powerful biological techniques for screening for catalytic activity. Matsui and Ulijn[124] applied phage display to identify hydrolytic peptides (Fig. 21). Several catalytically active peptides capable of promoting *p*-NPA hydrolysis as well as amide bond formation were identified in a random library of 10^9 12-residue peptides. Subsequent fusing of one of the catalytic peptides (CP4) to the core sequence of Aβ peptide resulted in additional 4-fold increase in catalytic efficiency of *p*-NPA hydrolysis upon self-assembly.[125] The activity of CP4-Aβ was attributed to formation of a Ser-His-Glu triad in the assembled state.[125, 126]

Self-assembling peptides can be adapted to form hybrid materials with carbon nanotubes (CNT). Covalent attachment of SHELKLKLKL, a catalytic triad mimicking hydrolytic peptide, and WLKLKLKL, a peptide designed to promote substrate association, to CNT produced catalytic materials capable of hydrolyzing *p*-NPA albeit with modest catalytic efficiency of 30–36 M^{-1} min^{-1} (Fig. 22).[127]

Histidine-based self-assembling hydrolases facilitate chemical reactions beyond hydrolysis of *p*-nitrophenol esters. Numata and co-workers[128] developed self-assembling peptides Ac-FFSGHFDFF-$CONH_2$ (PC3) and Ac-FGFHFSFDF-$CONH_2$ (PC4) that upon fibril formation hydrolyzed an amide bond in L-alanine-*p*-nitroanilide. Liu, Wang and co-workers demonstrated that assemblies of seven-residue peptides facilitate hydrolysis of cellobiose, a glucose dimer connected by a β-1,4-glycosidic bond.[129] Peptide PC5 (Ac-FEFEAEA-$CONH_2$) showing the highest activity under optimal conditions (pH 3.0, 25 °C) does not contain histidine residues, thus cellobiose hydrolysis must proceed via an alternative mechanism.

Self-assembled peptide catalysts with metal cofactors

Formation of large oligomeric structures in the presence of (or driven by) metal ion cofactors leads to highly efficient catalytic assemblies. Miravet and co-workers utilized self-assembly of pyridine-containing peptides **17** and **18** (Fig. 15) and $Pd(OAc)_2$ to produce gels capable of catalyzing benzylic alcohol oxidation. Interestingly, Pd(II) can be only functionally added after the gel was already formed.[130]

A nanotube produced by self-assembly of *N,N′*-hexadecanedioyl-di-L-glutamic acid in the presence of Cu(II) ions was reported in 2013 by Liu and co-workers.[131] The nanostructures function as an asymmetric catalyst for Diels-Alder cycloaddition between cyclopentadiene and aza-chalcone and provide a 92% yield after 24 hours, *dr* (*endo/exo*) of 95:5 in combination with a 47% *ee* (Scheme 5).

Very active self-assembling metallocatalysts can be designed *de novo* using basic principles. Short seven-residue peptide Fmoc-LKLKLKL-$CONH_2$ with alternating hydrophobic and hydrophilic residues forms β-sheet structure on the water-air interface.[132] We have modified the sequence of this peptide to incorporate a metal-binding site by substituting two of the lysines by histidines, all possible hydrophilic residues were tested in the remaining lysine position. The resulting peptide library was screened for the ability to catalyze hydrolysis of *p*-NPA in the presence of zinc. Several of the designed peptides showed high catalytic activity and subsequent structure-activity relationships established by mutagenesis of the original set of peptides allowed for further rational improvement to reach catalytic efficiency $(k_{cat}/K_M)_{max}$ of 19,200 M^{-1} min^{-1}.[133] This level of catalytic activity rivals those shown by natural hydrolytic enzymes by weight. Importantly, the active peptides form amyloid-like fibrils and their catalytic activity correlates with the degree of assembly, as monomeric peptides are essentially inactive in this reaction.

Mixing of peptides with different sequences allows for production of heterogeneous fibrils with multiple combinations of functional groups. In most cases this arrangement has a synergistic effect (positive or negative) and it allows for extremely high-throughput screening of peptide combinations to identify and further improve the most productive ones (Fig. 23).

Catalytic amyloids show very high homogeneity at the molecular level as evidenced by solid state NMR (ssNMR) experiments. This allowed us to determine the structure of the most active catalytic amyloid using ssNMR.[134] The backbone dihedrals were obtained through chemical shifts using TALOS+, the rotameric states of the coordinating histidine residues were obtained from Rotational-echo, double-resonance nuclear magnetic resonance (REDOR) experiments and the relative orientation of the strands was established using 2D ^{13}C-^{13}C correlation experiments. Interestingly, the structure showed a zig-zag pattern of zinc atoms connected by bridging histidines (Fig. 24, right). The bridging nature of histidines was additionally confirmed by measuring ^{15}N-^{1}H dipolar couplings. The structure was validated by statistical analysis of histidine rotamers on all reported structurally characterized zinc-containing proteins.

Zinc-containing catalytic amyloids show the ability to hydrolyze a wide range of various substrates from activated amino acid esters[135] to highly challenging phosphoesters such as paraoxon (Scheme 6, bottom right) by three orders of magnitude over the background rate.[136] Moreover, being essentially heterogeneous catalysts they can be easily deposited on various surfaces and exploited in flow devices enabling multiple passes of the reaction mixture over the catalyst.[136] Catalytic amyloids formed by Ac-LHLHLRL-$CONH_2$ and Ac-IHIHIQI-$CONH_2$ in the presence of Zn(II) preserve their structure in the wide range of pressures (0.1–400 MPa) and temperatures (20–60 °C). Moreover, the esterase activity of the fibrils increased up to 4-fold at higher temperatures and pressures. Interestingly, the K_M was practically not affected by the pressure increase, whereas both K_M and k_{cat} were affected by temperature change.[137]

Serpell and co-workers[138] showed that a peptide Ac-IHIHIYI-$CONH_2$ at pH 8 and in the presence of Zn(II) demonstrated impressive catalytic efficiency in *p*-NPA hydrolysis with reported k_{cat}/K_M values reaching 21,300 ± 900 M^{-1} min^{-1}. A structural model for the peptide assemblies was devised based on X-ray fiber diffraction (X-RFD) data (Fig. 25).

Catalytic amyloids can be produced using naturally occurring sequences. Fusing a highly conserved motif found in RNA polymerases (NADFDGD) to an amyloidogenic fragment QMAVHV yielded catalytic amyloids that can hydrolyze ATP with a k_{cat} value of 2.3 ± 0.2 × 10^{-4} min^{-1}, and catalytic efficiency of $k_{cat}/K_M = 3.3 \pm 0.22 \times 10^{-6}$ M^{-1} min^{-1} in a metal-dependent manner (Mg(II) or Mn(II)).[139]

The ability of catalytic amyloids to promote chemical reactions is not limited to hydrolysis. A generic nature of their metal coordination spheres allows for binding of other metal ions. Screening of a library of catalytic amyloids identified several peptides that efficiently promote redox-mediated dimerization of 2,6-dimethoxyphenol (DMP) in the presence of dioxygen and Cu(II) (Scheme 6, top). Formally this reaction proceeds via a C-H bond activation and C-C bond formation and thus it presents an exciting opportunity to expand on the catalytic repertoire of catalytic amyloids.[140]

Given copper's ability to promote hydrolytic reactions in addition to redox chemistry, catalytic amyloids containing Cu(II) promote cascade reactions. In a proof-of-concept experiment fluorescin diacetate was hydrolyzed and oxidized by copper-containing catalytic amyloids (Scheme 6, bottom left). Kinetic parameters of the reaction are consistent with two simultaneous processes without substrate dissociation between the two steps.[136]

Greenwald, Riek and co-workers took a comprehensive approach to identification of catalytic amyloids for productive catalysis.[141] Screening a large library of peptides with systematically varied sequences yielded a number of catalysts for *p*-NPA hydrolysis in the presence of zinc. Zinc coordination by His-X-His emerged as a motif that is crucial for catalysis. Interestingly, *p*-NPA hydrolysis was also observed at lower pH facilitated by peptides that do not possess the His-X-His motif suggesting a completely different mechanism of the reaction.

While His-X-His motif in peptides provides structure and rigidity associated with efficient catalysis, it is possible to promote chemical reactions using larger spacers. Lee and co-

workers showed that histidyl bolaamphiphilic molecule bis(*N*-α-amidohistidine)-1,7-heptane dicarboxylate self-assembles into "blob-like" structures with catalytic zinc sites (Fig. 26).[142]

The resulting assemblies catalyze *p*-NPA hydrolysis at pH 7 in the presence of 1 μM Zn(II) with catalytic efficiency (k_{cat}/K_M) of 79.2 M^{-1} min^{-1}. Additionally, they catalyze CO_2 hydration with catalytic efficiencies of 165, 413 and 661 M^{-1} min^{-1} at pH 7, 8 and 9, respectively.

The bolaamphiphilic assemblies can be modified to include fluorescent probes by co-assembling histidine and tyrosine-containing peptides.[143] The modified assemblies shared similar morphology as the parent ones, and were able to hydrolyze *p*-NPA with the same efficiency. The hydrolysis product quenched the tyrosine photoluminescence providing an additional handle for reaction monitoring and mechanistic studies.

Guler *et al.* reported that peptide amphiphiles with the sequence lauryl-VVAGHH-$CONH_2$ in the presence of Cu(II) self-assemble into nanofibers that catalyze a bioorthogonal click reaction.[144] The nanofiber showed the highest activity among all tested compounds (including L-histidine-copper complex reported as the most active in copper-catalyzed azide-alkyne cycloaddition (CuAAC) reactions) in click reaction between phenylacetylene and benzylazide at room temperature in water. Sequestration of copper by the self-assembled ligands reduced the toxicity of copper, making the catalyst biocompatible, as shown by efficient cell labeling.

Biocompatibility and catalytic properties of peptide amphilphiles can be applied to induce bone regeneration that relies on alkaline phosphatase activity.[145] Lauryl-VVAGHH-$CONH_2$ shows phosphatase activity using *p*-nitrophenyl phosphate (*p*-NPP) as a substrate with a k_{cat} value of 1.1×10^{-5} min^{-1}, and catalytic efficiency of 0.0414 M^{-1} min^{-1}. The nanofiber provides not only catalysis but serves as a bone-like nodule inducing scaffold. The nanofibers induce *in vitro* osteogenic differentiation without additional support (Fig. 27). A rapid maturation of osteoblast-like cells and mesenchymal stem cells (MSCs) into osteoblasts was observed.

Fry and coworkers employed simple peptide amphiphiles with the sequence palmitoyl-xyL_3K_3-CO_2H, where xy represents various residues constituting the heme binding region, to demonstrate that supramolecular assembly mode regulates the heme binding and consequently peroxidase activity of the resulting catalysts.[146] The amphiphiles contain positively charged trilysine headgroup that serves as a pH trigger capable of inducing fiber assembly. The palmitoyl moiety is included to promote hydrophobic collapse and the three leucine residues provide a β-sheet structural motif that favors the formation of long-aspect ratio nanofibers. The amphiphiles can produce assemblies of different morphologies in the presence of heme (fibrils *vs* micelles) depending on pH conditions. While heme is accessible to small molecules in both cases, significantly higher peroxidase activity was observed in heme-containing micelles (Fig. 28).

Interestingly, heme-based self-assembling catalytic structures can be obtained by mixing very simple building blocks such as Fmoc-protected phenylalanine and lysine with hemin.

The resulting gel promoted oxidation of pyrogallol to purpurogallin in either water or toluene (Scheme 7). Addition of the histidine to the structure leads to an additional synergistic increase in peroxidase activity from k_{cat} = 19.9 min^{-1} to 49.7 min^{-1}.[147]

Catalytic assemblies do not have to rely exclusively on peptides for self-assembly. Ding and co-workers reported the design of a catalytic heme-containing nanoparticle with peroxidase activity assembled from nucleic acid and peptide components.[148] The spherical nanoparticles produced by association of a long positively charged polyhistidine peptide (H_{32}) and folded guanine-rich DNAzyme-I (GGGTAGGGCGGGTTGGG; DzI) in the presence of hemin catalyze oxidization of ABTS (2,2′-azino-bis-(3-ethylbenzothiazoline-6-sulfonic acid)) by H_2O_2. The observed k_{cat} value of 180.6 min^{-1} is less than an order of magnitude lower that of horseradish peroxidase (approximately 1092 min^{-1}). The catalytic efficiency (k_{cat}/K_M) of the hemin-containing nanoparticle was almost identical to that of myoglobin.

4. Peptide self-replication

Autocatalytic templating and self-assembly of biologically relevant peptides has been an inspiration to the field. Indeed, if short peptides can promote catalytic reactions and template their own structure one can envision a highly efficient system capable for replicating and even evolving itself!

The first example of sequence specific replication reported by Ghadiri *et al.* took advantage of templated native chemical ligation. A 32-residue α-helical peptide was designed based on the leucine-zipper domain of the yeast transcription factor GCN4 to autocatalytically accelerate its own synthesis by condensation of 15- and 17-residue fragments in neutral, dilute aqueous solutions (Fig. 29).[149] Subsequent studies showed that the self-replicating system functions in a hypercyclic fashion wherein two or more self-replicating catalytic species cooperatively improve the other peptides production.[150, 151]

Self-replicating peptide sequences are not limited to α-helical structures. Ashkenasy and co-workers[152, 153] reported preferential self-replication of 12-residue peptides from short complementary structures (a 5-mer with a thioester and a 7-mer) in the presence of 12-residue template (Scheme 8). Moreover, when using mixtures of peptides with different stereochemistry, an enhanced formation of the one product (with the same stereochemistry) was observed. In the absence of fibrillating templates, a mixture of products with various morphologies and stereochemistry was formed and only two of them formed fibrils.[154]

Greenwald, Riek and co-workers showed that amyloid assemblies formed by short peptides can direct the sequence-selective, regioselective and stereoselective condensation of amino acids. The addition of activated racemic arginine and phenylalanine to the peptide RFRFR-$CONH_2$ in the presence of the complementary template peptide Ac-FEFEFEFE-$CONH_2$ selectively yields the product FRFRFRFR-$CONH_2$ with only L-stereochemistry (Fig. 30). In the absence of the template the reaction produced only single and double additions of mixed stereochemistry.[155]

The next logical step in development of self-replicating peptides is to attempt to do it on functional structures. Lynn and co-workers constructed a peptide K1 (Ac-KLVFFAE-$CONH_2$) using the nucleating core of Aβ peptide (LVFF). This peptide self-assembles into nanotube-like structures (Fig. 31) and demonstrates retroaldolase activity with a four-order of magnitude higher activity as compared to lysine alone. Subsequent sequence modification that results in subtle structural morphological changes provided additional rate acceleration (up to 10-fold) in the stereoselective conversion of methodol to fluorescent 6-amino-2-naphthaldehyde.[156] Templating additional stages of polymer synthesis using the methodology developed in the Lynn lab[157] is likely to enable construction of more efficient catalytic materials.

5. Conclusions

The idea that multiple molecules can come together in a predetermined fashion to produce an assembly with emerging catalytic properties is truly fascinating. Peptides have been at the forefront of experimental validation of this concept due to availability of extremely chemically versatile building blocks, simplicity of synthesis, and access to multiple secondary, tertiary, etc. structures. Much effort has been dedicated to establishing the basic principles that would allow at least somewhat accurate prediction of molecular structures that can accomplish this feat. Early successes in the field almost exclusively were based on discreet, well-defined and readily characterizable structures that fold in a very predictable manner. Especially in the presence of metal cofactors, such peptide assemblies showed substantial increase in catalytic activity over the rate of uncatalyzed reaction. However, having the peptide designed to fold in a specific and very stable fold imposes constraints on the sequence. Besides, is our understanding of catalysis sufficient to predict the structure of a perfect catalyst *de novo*? Multiple failures of computational tools to achieve high rate of catalysis while getting the designed structure with subatomic precision suggests otherwise. Thus, advances of the past decade have been linked with a very minimalist approach, which can be summarized in the following way. Let's introduce very basic catalytic handles into a structure prone to self-assembly and let the chips fall where they may. Despite the seeming naiveté this concept has been extremely successful. The relatively short sequences of peptides employed in such assemblies allow for rapid screening of a large number of possibilities and establishing meaningful structure activity relationships that can be used to improve upon the existing catalysts *rationally*. Additionally, the non-covalent nature of the assemblies allows for mixing peptides with different sequences providing even higher throughput opportunities in addition to possibilities to evolve via self-replication. Advances in the field are aided by improved characterization techniques – the ongoing explosive expansion of cryoelectron microscopy and ssNMR provides insight simply impossible to obtain just a few decades ago. More is undoubtedly to come. Composite materials that contain nanoparticles[158–172] and dendrimers offer additional functional advantages.[173] While most of reactions described above are considered to be model (and for which there are traditional catalysts available) there is every expectation that new highly efficient self-assembling catalytic materials will be soon available for industrially relevant processes. Robustness, heterogeneity, low cost and potential ability to self-replicate will undoubtedly make them a popular tool in a chemists' toolbox.

Acknowledgments

We thank Prof. Olga V. Makhlynets for her comments. This work was supported by the NIH (Grant No. GM119634 to I.V.K.), the NSF (Grant No. 1332349 to I.V.K.), the ORAU Ralph E. Powe Award to I.V.K. and the Alexander von Humboldt Foundation.

References

1. Lewis NS, Nocera DG. Proc Natl Acad Sci USA. 2006; 103:15729–15735. [PubMed: 17043226]
2. Korendovych IV, DeGrado WF. Curr Opin Struct Biol. 2014; 27:113–121. [PubMed: 25048695]
3. Ghosh I, Chmielewski J. Curr Opin Chem Biol. 2004; 8:640–644. [PubMed: 15556409]
4. Miller SL, Urey HC. Science. 1959; 130:245–251. [PubMed: 13668555]
5. Danger G, Plasson R, Pascal R. Chem Soc Rev. 2012; 41:5416–5429. [PubMed: 22688720]
6. Jakschitz TA, Rode BM. Chem Soc Rev. 2012; 41:5484–5489. [PubMed: 22733315]
7. Rode BM. Peptides. 1999; 20:773–786. [PubMed: 10477135]
8. Carny O, Gazit E. FASEB J. 2005; 19:1051–1055. [PubMed: 15985527]
9. Greenwald J, Friedmann MP, Riek R. Angew Chem, Int Ed Engl. 2016; 55:11609–11613. [PubMed: 27511635]
10. Greenwald J, Riek R. Structure. 2010; 18:1244–1260. [PubMed: 20947013]
11. Greenwald J, Riek R. J Mol Biol. 2012; 421:417–426. [PubMed: 22542525]
12. Griswold KS, Miller SJ. Tetrahedron. 2003; 59:8869–8875.
13. Peris G, Jakobsche CE, Miller SJ. J Am Chem Soc. 2007; 129:8710–8711. [PubMed: 17592849]
14. Kolundzic F, Noshi MN, Tjandra M, Movassaghi M, Miller SJ. J Am Chem Soc. 2011; 133:9104–9111. [PubMed: 21539386]
15. Boncheva M, Whitesides GM. Mrs Bull. 2005; 30:736–742.
16. Mendes AC, Baran ET, Reis RL, Azevedo HS. WIREs Nanomed Nanobiotechnol. 2013; 5:582–612.
17. Lupas A. Trends Biochem Sci. 1996; 21:375–382. [PubMed: 8918191]
18. Woolfson DN. Advances in protein chemistry. 2005; 70:79–112. [PubMed: 15837514]
19. Issac R, Ham YW, Chmielewski J. Curr Opin Struct Biol. 2001; 11:458–463. [PubMed: 11495739]
20. Leman LJ, Weinberger DA, Huang ZZ, Wilcoxen KM, Ghadiri MR. J Am Chem Soc. 2007; 129:2959–2966. [PubMed: 17302417]
21. Cavalli S, Albericio F, Kros A. Chem Soc Rev. 2010; 39:241–263. [PubMed: 20023851]
22. Cherny I, Gazit E. Angew Chem, Int Ed Engl. 2008; 47:4062–4069. [PubMed: 18412209]
23. Bowerman CJ, Nilsson BL. Biopolymers. 2012; 98:169–184. [PubMed: 22782560]
24. Du X, Zhou J, Shi J, Xu B. Chem Rev. 2015; 115:13165–13307. [PubMed: 26646318]
25. Gao Y, Zhao F, Wang Q, Zhang Y, Xu B. Chem Soc Rev. 2010; 39:3425–3433. [PubMed: 20623068]
26. Fichman G, Gazit E. Acta Biomater. 2014; 10:1671–1682. [PubMed: 23958781]
27. Rasale DB, Das AK. Int J Mol Sci. 2015; 16:10797–10820. [PubMed: 25984603]
28. Zhang S. Nat Biotechnol. 2003; 21:1171–1178. [PubMed: 14520402]
29. Zhao XB, Pan F, Lu JR. Prog Nat Sci: Mater Int. 2008; 18:653–660.
30. Habibi N, Kamaly N, Memic A, Shafiee H. Nano Today. 2016; 11:41–60. [PubMed: 27103939]
31. Escuder B, Rodriguez-Llansola F, Miravet JF. New J Chem. 2010; 34:1044–1054.
32. Miravet JF, Escuder B. Rsc Soft Matter Ser. 2014; 1:117–156.
33. Singh N, Kumar M, Miravet JF, Ulijn RV, Escuder B. Chem Eur J. 2017; 23:981–993. [PubMed: 27530095]
34. Singh N, Tena-Solsona M, Miravet JF, Escuder B. Isr J Chem. 2015; 55:711–723.
35. Wang W, Anderson CF, Wang Z, Wu W, Cui H, Liu CJ. Chem Sci. 2017; 8:3310–3324. [PubMed: 28507701]

36. Johnsson K, Allemann RK, Widmer H, Benner SA. Nature. 1993; 365:530–532. [PubMed: 8413606]
37. Broo KS, Brive L, Ahlberg P, Baltzer L. J Am Chem Soc. 1997; 119:11362–11372.
38. Broo KS, Nilsson H, Nilsson J, Baltzer L. J Am Chem Soc. 1998; 120:10287–10295.
39. Broo KS, Nilsson H, Nilsson J, Flodberg A, Baltzer L. J Am Chem Soc. 1998; 120:4063–4068.
40. Baltzer L, Broo KS, Nilsson H, Nilsson J. Bioorg Med Chem. 1999; 7:83–91. [PubMed: 10199659]
41. Razkin J, Nilsson H, Baltzer L. J Am Chem Soc. 2007; 129:14752–14758. [PubMed: 17985898]
42. Razkin J, Lindgren J, Nilsson H, Baltzer L. ChemBioChem. 2008; 9:1975–1984. [PubMed: 18600814]
43. Allert M, Baltzer L. ChemBioChem. 2003; 4:306–318. [PubMed: 12672110]
44. Baumeister B, Matile S. Chem Eur J. 2000; 6:1739–1749. [PubMed: 10845631]
45. Baumeister B, Sakai N, Matile S. Angew Chem Int Ed. 2000; 39:1955–1958.
46. Baumeister B, Sakai N, Matile S. Org lett. 2001; 3:4229–4232. [PubMed: 11784184]
47. Sakai N, Sordé N, Matile S. J Am Chem Soc. 2003; 125:7776–7777. [PubMed: 12822976]
48. Baumeister B, Matile S. Macromolecules. 2002; 35:1549–1555.
49. Som A, Matile S. Eur J Org Chem. 2002; 2002:3874–3883.
50. Das G, Talukdar P, Matile S. Science. 2002; 298:1600–1602. [PubMed: 12446904]
51. Fuentes JA, Lebl T, Slawin AMZ, Clarke ML. Chem Sci. 2011; 2:1997–2005.
52. Makhlynets OV, Korendovych IV. Nat Chem. 2016; 8:823–824. [PubMed: 27554407]
53. Burton AJ, Thomson AR, Dawson WM, Brady RL, Woolfson DN. Nat Chem. 2016; 8:837–844. [PubMed: 27554410]
54. Moroz YS, Dunston TT, Makhlynets OV, Moroz OV, Wu Y, Yoon JH, Olsen AB, McLaughlin JM, Mack KL, Gosavi PM, van Nuland NAJ, Korendovych IV. J Am Chem Soc. 2015; 137:14905–14911. [PubMed: 26555770]
55. Marsh EN, DeGrado WF. Proc Natl Acad Sci USA. 2002; 99:5150–5154. [PubMed: 11959963]
56. Kaplan J, DeGrado WF. Proc Natl Acad Sci USA. 2004; 101:11566–11570. [PubMed: 15292507]
57. Reig AJ, Pires MM, Snyder RA, Wu Y, Jo H, Kulp DW, Butch SE, Calhoun JR, Szyperski T, Solomon EI, DeGrado WF. Nat Chem. 2012; 4:900. [PubMed: 23089864]
58. Ulas G, Lemmin T, Wu YB, Gassner GT, DeGrado WF. Nat Chem. 2016; 8:354–359. [PubMed: 27001731]
59. Chakraborty S, Yudenfreund Kravitz J, Thulstrup PW, Hemmingsen L, DeGrado WF, Pecoraro VL. Angew Chem, Int Ed. 2011; 50:2049–2053.
60. Iranzo O, Chakraborty S, Hemmingsen L, Pecoraro VL. J Am Chem Soc. 2010; 133:239–251. [PubMed: 21162521]
61. Chakraborty S, Touw DS, Peacock AFA, Stuckey J, Pecoraro VL. J Am Chem Soc. 2010; 132:13240–13250. [PubMed: 20825181]
62. Zastrow ML, Peacock AFA, Stuckey JA, Pecoraro VL. Nat Chem. 2011; 4:118. [PubMed: 22270627]
63. Zastrow ML, Pecoraro VL. J Am Chem Soc. 2013; 135:5895–5903. [PubMed: 23516959]
64. Zhu Y, Alonso DO, Maki K, Huang CY, Lahr SJ, Daggett V, Roder H, DeGrado WF, Gai F. Proc Natl Acad Sci USA. 2003; 100:15486–15491. [PubMed: 14671331]
65. Cangelosi VM, Deb A, Penner-Hahn JE, Pecoraro VL. Angew Chem, Int Ed. 2014; 53:7900–7903.
66. Tegoni M, Yu F, Bersellini M, Penner-Hahn JE, Pecoraro VL. Proc Natl Acad Sci USA. 2012; 109:21234–21239. [PubMed: 23236170]
67. Wijma HJ, Jeuken LJC, Verbeet MP, Armstrong FA, Canters GW. J Biol Chem. 2006; 281:16340–16346. [PubMed: 16613859]
68. Choma CT, Lear JD, Nelson MJ, Dutton PL, Robertson DE, DeGrado WF. J Am Chem Soc. 1994; 116:856–865.
69. Korendovych IV, Senes A, Kim YH, Lear JD, Fry HC, Therien MJ, Blasie JK, Walker FA, Degrado WF. J Am Chem Soc. 2010; 132:15516–15518. [PubMed: 20945900]

70. Mahajan M, Bhattacharjya S. Angew Chem, Int Ed. 2013; 52:6430–6434.
71. Watkins DW, Jenkins JM, Grayson KJ, Wood N, Steventon JW, Le Vay KK, Goodwin MI, Mullen AS, Bailey HJ, Crump MP. Nat Commun. 2017; 8:358. [PubMed: 28842561]
72. Gibney BR, Rabanal F, Dutton PL. Curr Opin Chem Biol. 1997; 1:537–542. [PubMed: 9667893]
73. Laungani AC, Slattery JM, Krossing I, Breit B. Chem Eur J. 2008; 14:4488–4502. [PubMed: 18449870]
74. Der BS, Edwards DR, Kuhlman B. Biochemistry. 2012; 51:3933–3940. [PubMed: 22510088]
75. Song WJ, Tezcan FA. Science. 2014; 346:1525–1528. [PubMed: 25525249]
76. Song WJ, Yu J, Tezcan FA. J Am Chem Soc. 2017; 139:16772–16779. [PubMed: 28992705]
77. Goodman CM, Choi S, Shandler S, DeGrado WF. Nat Chem Biol. 2007; 3:252–262. [PubMed: 17438550]
78. Cheng RP, Gellman SH, DeGrado WF. Chem Rev. 2001; 101:3219–3232. [PubMed: 11710070]
79. Korendovych IV, Kim YH, Ryan AH, Lear JD, DeGrado WF, SSJ. Org Lett. 2010; 12:5142–5145. [PubMed: 20945888]
80. Korendovych IV, Shandler SJ, Montalvo GL, DeGrado WF. Org Lett. 2011; 13:3474–3477. [PubMed: 21651308]
81. Daniels DS, Petersson EJ, Qiu JX, Schepartz A. J Am Chem Soc. 2007; 129:1532–1533. [PubMed: 17283998]
82. Qiu JX, Petersson EJ, Matthews EE, Schepartz A. J Am Chem Soc. 2006; 128:11338–11339. [PubMed: 16939241]
83. Shandler SJ, Korendovych IV, Moore DT, Dupont-Smith KB, Streu CN, Litvinov RI, Billings PC, Gai F, Bennett JS, DeGrado WF. J Am Chem Soc. 2011; 133:12378–12381. [PubMed: 21780757]
84. Müller MM, Windsor MA, Pomerantz WC, Gellman SH, Hilvert D. Angew Chem. 2009; 121:940–943.
85. Jiang L, Althoff EA, Clemente FR, Doyle L, Rothlisberger D, Zanghellini A, Gallaher JL, Betker JL, Tanaka F, Barbas CF 3rd, Hilvert D, Houk KN, Stoddard BL, Baker D. Science. 2008; 319:1387–1391. [PubMed: 18323453]
86. Wang PS, Nguyen JB, Schepartz A. J Am Chem Soc. 2014; 136:6810–6813. [PubMed: 24802883]
87. List B, Lerner RA, Barbas CF. J Am Chem Soc. 2000; 122:2395–2396.
88. Northrup AB, MacMillan DWC. J Am Chem Soc. 2002; 124:6798–6799. [PubMed: 12059180]
89. Tan R, Li C, Luo J, Kong Y, Zheng W, Yin D. J Catal. 2013; 298:138–147.
90. List B, Pojarliev P, Biller WT, Martin HJ. J Am Chem Soc. 2002; 124:827–833. [PubMed: 11817958]
91. Marques MMB. Angew Chem, Int Ed. 2006; 45:348–352.
92. List B, Pojarliev P, Martin HJ. Org Lett. 2001; 3:2423–2425. [PubMed: 11483025]
93. Andrey O, Alexakis A, Bernardinelli G. Org Lett. 2003; 5:2559–2561. [PubMed: 12841780]
94. Hayashi Y, Yamaguchi J, Sumiya T, Shoji M. Angew Chem. 2004; 116:1132–1135.
95. Vignola N, List B. J Am Chem Soc. 2004; 126:450–451. [PubMed: 14719926]
96. Ahrendt KA, Borths CJ, MacMillan DW. J Am Chem Soc. 2000; 122:4243–4244.
97. Rodriguez-Llansola F, Escuder B, Hamley IW, Hayes W, Miravet JF. Soft Matter. 2012; 8:8865–8872.
98. Diaz-Oltra S, Berdugo C, Miravet JF, Escuder B. New J Chem. 2015; 39:3785–3791.
99. Rodriguez-Llansola F, Escuder B, Miravet JF. J Am Chem Soc. 2009; 131:11478–11484. [PubMed: 19459635]
100. Rodriguez-Llansola F, Escuder B, Miravet JF. Org Biomol Chem. 2009; 7:3091–3094.
101. Rodriguez-Llansola F, Miravet JF, Escuder B. Chem Commun. 2009:7303–7305.
102. Rodriguez-Llansola F, Miravet JF, Escuder B. Chem Eur J. 2010; 16:8480–8486. [PubMed: 20540050]
103. Singh N, Escuder B. Chem Eur J. 2017; 23:9946–9951. [PubMed: 28513914]
104. Berdugo C, Miravet JF, Escuder B. Chem Commun. 2013; 49:10608–10610.

105. Singh N, Zhang K, Angulo-Pachon CA, Mendes E, van Esch JH, Escuder B. Chem Sci. 2016; 7:5568–5572.
106. Soares BM, Aguilar AM, Silva ER, Coutinho-Neto MD, Hamley IW, Reza M, Ruokolainen J, Alves WA. Phys Chem Chem Phys. 2017; 19:1181–1189. [PubMed: 27942644]
107. Tena-Solsona M, Nanda J, Diaz-Oltra S, Chotera A, Ashkenasy G, Escuder B. Chem Eur J. 2016; 22:6687–6694. [PubMed: 27004623]
108. Mingzhe S, Qingxian J, Li Z, Minghua L. Chem Lett. 2012; 41:1349–1350.
109. Qin L, Zhang L, Jin Q, Zhang J, Han B, Liu M. Angew Chem, Int Ed. 2013; 52:7761–7765.
110. Lee KS, Parquette JR. Chem Commun. 2015; 51:15653–15656.
111. Guler MO, Stupp SI. J Am Chem Soc. 2007; 129:12082–12083. [PubMed: 17854188]
112. Singh N, Conte MP, Ulijn RV, Miravet JF, Escuder B. Chem Commun. 2015; 51:13213–13216.
113. Belieres M, Chouini-Lalanne N, Dejugnat C. RSC Adv. 2015; 5:35830–35842.
114. Huang ZP, Guan SW, Wang YG, Shi GN, Cao LN, Gao YZ, Dong ZY, Xu JY, Luo Q, Liu JQ. J Mater Chem B. 2013; 1:2297–2304.
115. Zhang GH, Huang RL, Qi W, Wang YF, Su RX, He ZM. RSC Adv. 2016; 6:40828–40834.
116. Wang M, Lv Y, Liu X, Qi W, Su R, He Z. ACS Appl Mater Interfaces. 2016; 8:14133–14141. [PubMed: 27191381]
117. Gulseren G, Khalily MA, Tekinay AB, Guler MO. J Mater Chem B. 2016; 4:4605–4611.
118. Garcia AM, Kurbasic M, Kralj S, Melchionna M, Marchesan S. Chem Commun. 2017; 53:8110–8113.
119. Zhang C, Xue X, Luo Q, Li Y, Yang K, Zhuang X, Jiang Y, Zhang J, Liu J, Zou G, Liang XJ. ACS Nano. 2014; 8:11715–11723. [PubMed: 25375351]
120. Zhang C, Shafi R, Lampel A, MacPherson D, Pappas CG, Narang V, Wang T, Maldarelli C, Ulijn RV. Angew Chem, Int Ed Engl. 2017; 56:14511–14515. [PubMed: 28941038]
121. Schneider JP, Pochan DJ, Ozbas B, Rajagopal K, Pakstis L, Kretsinger J. J Am Chem Soc. 2002; 124:15030–15037. [PubMed: 12475347]
122. Haines-Butterick L, Rajagopal K, Branco M, Salick D, Rughani R, Pilarz M, Lamm MS, Pochan DJ, Schneider JP. Proc Natl Acad Sci USA. 2007; 104:7791–7796. [PubMed: 17470802]
123. Nagy-Smith K, Beltramo PJ, Moore E, Tycko R, Furst EM, Schneider JP. ACS Cent Sci. 2017; 3:586–597. [PubMed: 28691070]
124. Maeda Y, Javid N, Duncan K, Birchall L, Gibson KF, Cannon D, Kanetsuki Y, Knapp C, Tuttle T, Ulijn RV, Matsui H. J Am Chem Soc. 2014; 136:15893–15896. [PubMed: 25343575]
125. Maeda Y, Fang J, Ikezoe Y, Pike DH, Nanda V, Matsui H. PLoS One. 2016; 11:e0153700. [PubMed: 27116246]
126. Maeda Y, Wei ZY, Ikezoe Y, Matsui H. Chemnanomat. 2015; 1:319–323.
127. Zhang Q, He X, Han A, Tu Q, Fang G, Liu J, Wang S, Li H. Nanoscale. 2016; 8:16851–16856. [PubMed: 27714071]
128. Wong YM, Masunaga H, Chuah JA, Sudesh K, Numata K. Biomacromolecules. 2016; 17:3375–3385. [PubMed: 27642764]
129. He XX, Zhang FY, Zhang L, Zhang Q, Fang GZ, Liu JF, Wang S, Zhang SQ. J Mater Chem B. 2017; 5:5225–5233.
130. Miravet JF, Escuder B. Chem Commun. 2005:5796–5798.
131. Jin Q, Zhang L, Cao H, Wang T, Zhu X, Jiang J, Liu M. Langmuir. 2011; 27:13847–13853. [PubMed: 21978005]
132. DeGrado WF, Lear JD. J Am Chem Soc. 1985; 107:7684.
133. Rufo CM, Moroz YS, Moroz OV, Stohr J, Smith TA, Hu X, DeGrado WF, Korendovych IV. Nat Chem. 2014; 6:303–309. [PubMed: 24651196]
134. Lee M, Wang T, Makhlynets OV, Wu Y, Polizzi NF, Wu H, Gosavi PM, Stohr J, Korendovych IV, DeGrado WF, Hong M. Proc Natl Acad Sci USA. 2017; 114:6191–6196. [PubMed: 28566494]
135. Heier JL, Mikolajczak DJ, Bottcher C, Koksch B. Biopolymers. 2017:108.
136. Lengyel Z, Rufo CM, Moroz YS, Makhlynets OV, Korendovych IV. ACS Catal. 2017:59–62.

137. Luong TQ, Erwin N, Neumann M, Schmidt A, Loos C, Schmidt V, Fändrich M, Winter R. Angewandte Chemie International Edition. 2016; 55:12412–12416. [PubMed: 27573584]
138. Al-Garawi ZS, McIntosh BA, Neill-Hall D, Hatimy AA, Sweet SM, Bagley MC, Serpell LC. Nanoscale. 2017; 9:10773–10783. [PubMed: 28722055]
139. Monasterio O, Nova E, Diaz-Espinoza R. Biochem Biophys Res Commun. 2017; 482:1194–1200. [PubMed: 27923655]
140. Makhlynets OV, Gosavi PM, Korendovych IV. Angew Chem, Int Ed. 2016; 55:9017–9020.
141. Friedmann MP, Torbeev V, Zelenay V, Sobol A, Greenwald J, Riek R. PLoS One. 2015; 10:e0143948. [PubMed: 26650386]
142. Kim MC, Lee SY. Chem Eur J. 2014; 20:17019–17024. [PubMed: 25332095]
143. Kwak J, Kim MC, Lee SY. ACS Appl Mater Interfaces. 2015; 7:14150–14156. [PubMed: 26052625]
144. Khalily MA, Gulseren G, Tekinay AB, Guler MO. Bioconjugate Chem. 2015; 26:2371–2375.
145. Gulseren G, Yasa IC, Ustahuseyin O, Tekin ED, Tekinay AB, Guler MO. Biomacromolecules. 2015; 16:2198–2208. [PubMed: 26039144]
146. Solomon LA, Kronenberg JB, Fry HC. J Am Chem Soc. 2017; 139:8497–8507. [PubMed: 28505436]
147. Wang Q, Yang Z, Zhang X, Xiao X, Chang CK, Xu B. Angew Chem, Int Ed Engl. 2007; 46:4285–4289. [PubMed: 17443763]
148. Liu Q, Wang H, Shi X, Wang ZG, Ding B. ACS Nano. 2017; 11:7251–7258. [PubMed: 28657711]
149. Lee DH, Granja JR, Martinez JA, Severin K, Ghadiri MR. Nature. 1996; 382:525–528. [PubMed: 8700225]
150. Lee DH, Severin K, Ghadiri MR. Curr Opin Chem Biol. 1997; 1:491–496. [PubMed: 9667892]
151. Lee DH, Severin K, Yokobayashi Y, Ghadiri MR. Nature. 1997; 390:591–594. [PubMed: 9403686]
152. Rubinov B, Wagner N, Rapaport H, Ashkenasy G. Angew Chem, Int Ed Engl. 2009; 48:6683–6686. [PubMed: 19644990]
153. Rubinov B, Wagner N, Matmor M, Regev O, Ashkenasy N, Ashkenasy G. ACS Nano. 2012; 6:7893–7901. [PubMed: 22856322]
154. Nanda J, Rubinov B, Ivnitski D, Mukherjee R, Shtelman E, Motro Y, Miller Y, Wagner N, Cohen-Luria R, Ashkenasy G. Nat Commun. 2017; 8:434. [PubMed: 28874657]
155. Rout SK, Friedmann MP, Riek R, Greenwald J. Nat Commun. 2018; 9:234. [PubMed: 29339755]
156. Omosun TO, Hsieh MC, Childers WS, Das D, Mehta AK, Anthony NR, Pan T, Grover MA, Berland KM, Lynn DG. Nat Chem. 2017; 9:805–809. [PubMed: 28754939]
157. Chen CR, Tan JJ, Hsieh MC, Pan T, Goodwin JT, Mehta AK, Grover MA, Lynn DG. Nat Chem. 2017; 9:799–804. [PubMed: 28754943]
158. Pengo P, Baltzer L, Pasquato L, Scrimin P. Angew Chem Int Ed. 2007; 46:400–404.
159. Zaramella D, Scrimin P, Prins LJ. J Am Chem Soc. 2012; 134:8396–8399. [PubMed: 22559143]
160. Zaramella D, Scrimin P, Prins LJ. Int J Mol Sci. 2013; 14:2011–2021. [PubMed: 23337201]
161. Tang C, Smith AM, Collins RF, Ulijn RV, Saiani A. Langmuir. 2009; 25:9447–9453. [PubMed: 19537819]
162. Nalluri SK, Shivarova N, Kanibolotsky AL, Zelzer M, Gupta S, Frederix PW, Skabara PJ, Gleskova H, Ulijn RV. Langmuir. 2014; 30:12429–12437. [PubMed: 25259412]
163. Frederix PW, Scott GG, Abul-Haija YM, Kalafatovic D, Pappas CG, Javid N, Hunt NT, Ulijn RV, Tuttle T. Nat Chem. 2015; 7:30–37. [PubMed: 25515887]
164. Pappas CG, Sasselli IR, Ulijn RV. Angew Chem, Int Ed Engl. 2015; 54:8119–8123. [PubMed: 26014441]
165. Scott G, Roy S, Abul-Haija YM, Fleming S, Bai S, Ulijn RV. Langmuir. 2013; 29:14321–14327. [PubMed: 24144273]
166. Zhou B, Sun Z, Li D, Zhang T, Deng L, Liu YN. Nanoscale. 2013; 5:2669–2673. [PubMed: 23463381]

167. Batzli KM, Love BJ. Mater Sci Eng C Mater Biol Appl. 2015; 48:103–111. [PubMed: 25579902]
168. Pan YX, Cong HP, Men YL, Xin S, Sun ZQ, Liu CJ, Yu SH. ACS Nano. 2015; 9:11258–11265. [PubMed: 26473307]
169. Maity I, Rasale DB, Das AK. RSC Adv. 2014; 4:2984–2988.
170. Hu Y, Xu W, Li G, Xu L, Song A, Hao J. Langmuir. 2015; 31:8599–8605. [PubMed: 26177269]
171. Xu W, Hong Y, Hu Y, Hao J, Song A. Chemphyschem. 2016; 17:2157–2163. [PubMed: 27028550]
172. Hickling C, Toogood HS, Saiani A, Scrutton NS, Miller AF. Macromol Rapid Commun. 2014; 35:868–874. [PubMed: 24604676]
173. Darbre T, Reymond JL. Acc Chem Res. 2006; 39:925–934. [PubMed: 17176031]

Biographies

Oleksii Zozulia was born in 1988 in Kharkiv, Ukraine. In 2010 he graduated in Chemistry at Kharkiv V. N. Karazin National University under the supervision of Prof. Dr. Andrey O. Doroshenko. In 2013 he joined the research group of Prof. Dr. Andriy Mokhir in Germany at the University of Erlangen-Nuremberg, where he obtained his PhD in 2017. He then moved to Syracuse University, US where he currently works as a Postdoctoral Researcher under the guidance of Prof. Dr. Ivan Korendovych. His most recent research interests are: peptide and protein catalytic assemblies, DNA/RNA-controlled chemical reactions and organic synthetic chemistry.

Martin A. Dolan was born in 1991 in Chicago, Illinois. He received his bachelor's degree in Biochemistry from Ramapo College of New Jersey in 2014. He is currently a PhD student working for Prof. Dr. Ivan Korendovych in the Chemistry department at Syracuse University. Martin spent his first two years of research at Syracuse University in Dr. Daniel Clark's organic and organometallic laboratory wherein he developed new ruthenium catalysts for ring-closing enyne metathesis. His research interests include synthetic organic chemistry and its applications to biochemistry, drug development, and medicinal chemistry.

Dr. Ivan V. Korendovych is an Associate Professor of Chemistry at Syracuse University. He received his B.S. and M.S. degrees in inorganic chemistry from the National Taras Shevchenko University of Kyiv and his Ph.D. degree from Tufts University working on mechanistic aspects of oxygen activation and anion recognition in the lab of Professor Elena Rybak-Akimova. After postdoctoral studies in the lab of Professor William DeGrado at the University of Pennsylvania School of Medicine Dr. Korendovych joined the faculty at Syracuse University in 2011. The main foci of Korendovych Lab include protein design and engineering, development of probes for cancer imaging, and medicinal chemistry. Prof. Korendovych is a recipient of many awards including an Alexander von Humboldt Research Fellowship, an ACS Division of Inorganic Chemistry Young Investigator Award and ORAU Ralph E. Powe Junior Faculty Award.

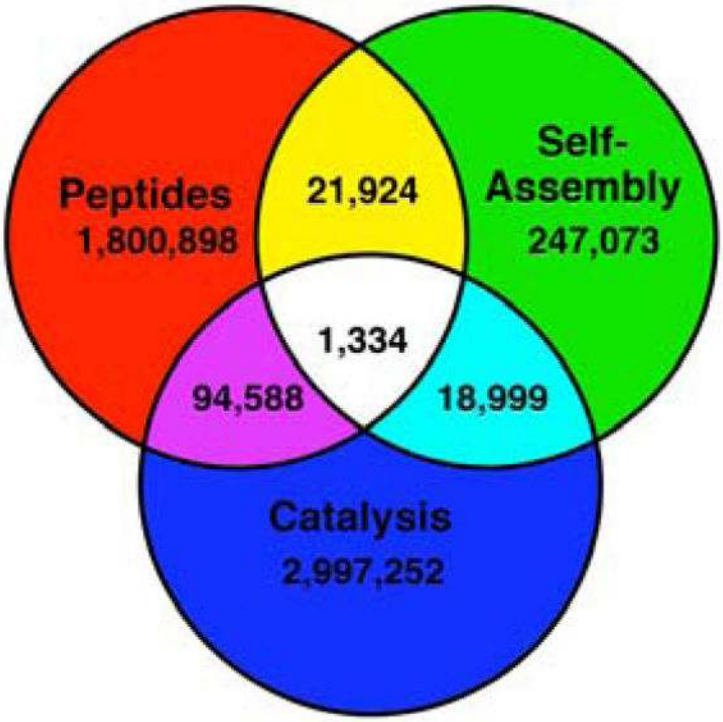

Figure 1.
Number of references produced in response to keyword queries of “peptides”, “self-assembly”, and “catalysis” as well as their overlaps returned by SciFinder on March 5th, 2018.

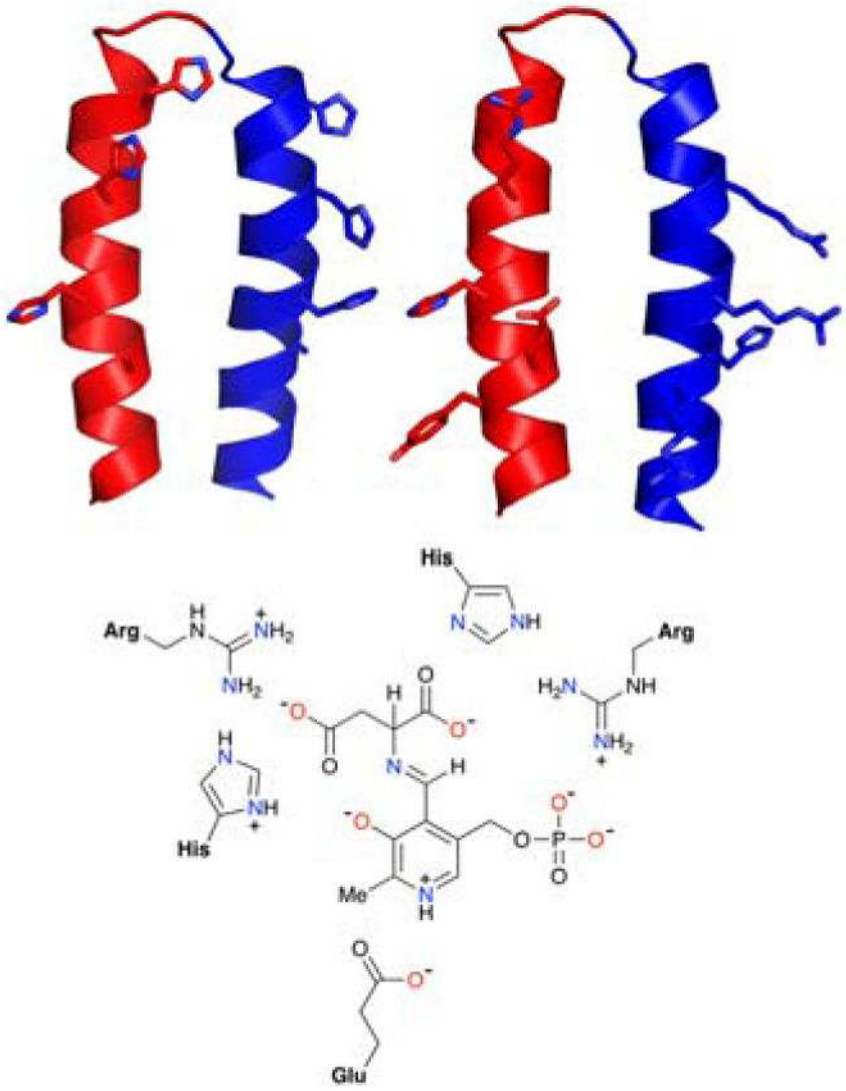

Figure 2.

(Top left) Representative model of helix-loop-helix peptide KO-42 showing the catalytically active histidines. (Top right) Representative model of T-16, a modified variant to KO-42 peptide, with corresponding mutations. Only side chains of the residues used for catalyst optimization are shown. (Bottom) Interactions designed to promote aldimine binding by T-4 and T-16.

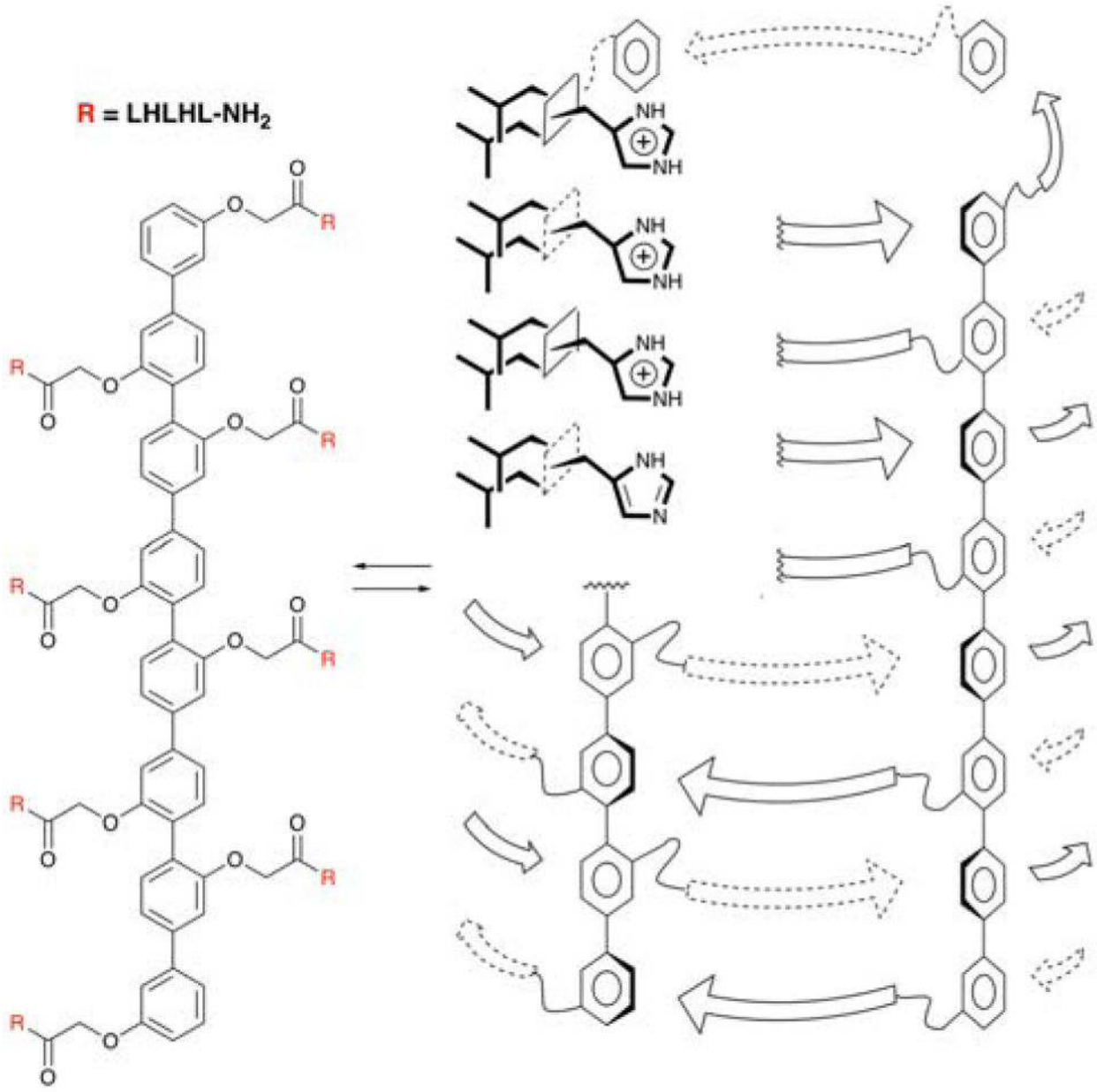

Figure 3.

A model of rigid-rod supramolecular β-barrels. Reproduced from ref. 46 with permission from the American Chemical Society, copyright 2001.

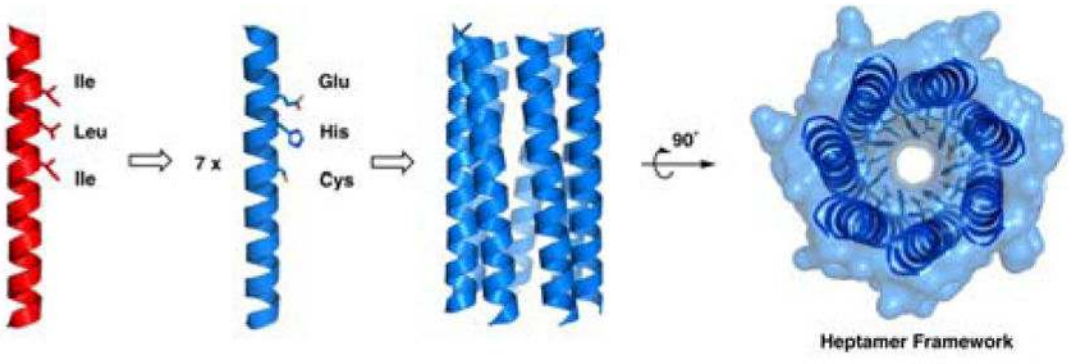

Figure 4.

Artificial esterase based on heptameric assembly of α-helical peptides. Glutamic acid, histidine, and cysteine were introduced into a previously reported non-catalytic self-assembling peptide (red) to produce a mutant (blue) that self-assembles into catalytic heptameric structure (PDB code 5EZC for an X-ray crystal structure of the heptamer).

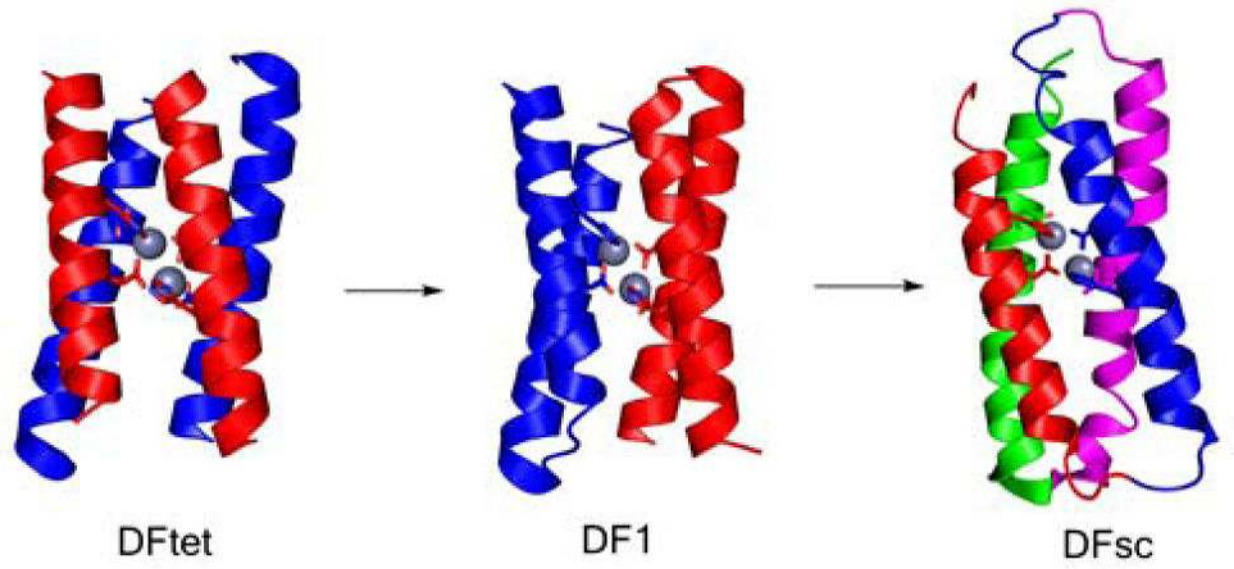

Figure 5.

Evolution of metallopeptide designs. The original DFtet, a heterotetrameric assembly, serves as a starting point for development of DF1, a homodimer of two helix-loop-helix subunits. DFsc is a single chain protein that is based on DF1. The structure of DF1 was determined by X-ray crystallography (PDB code 1JMB), the structure of DFsc was determined by NMR (PDB code 2HZ8).

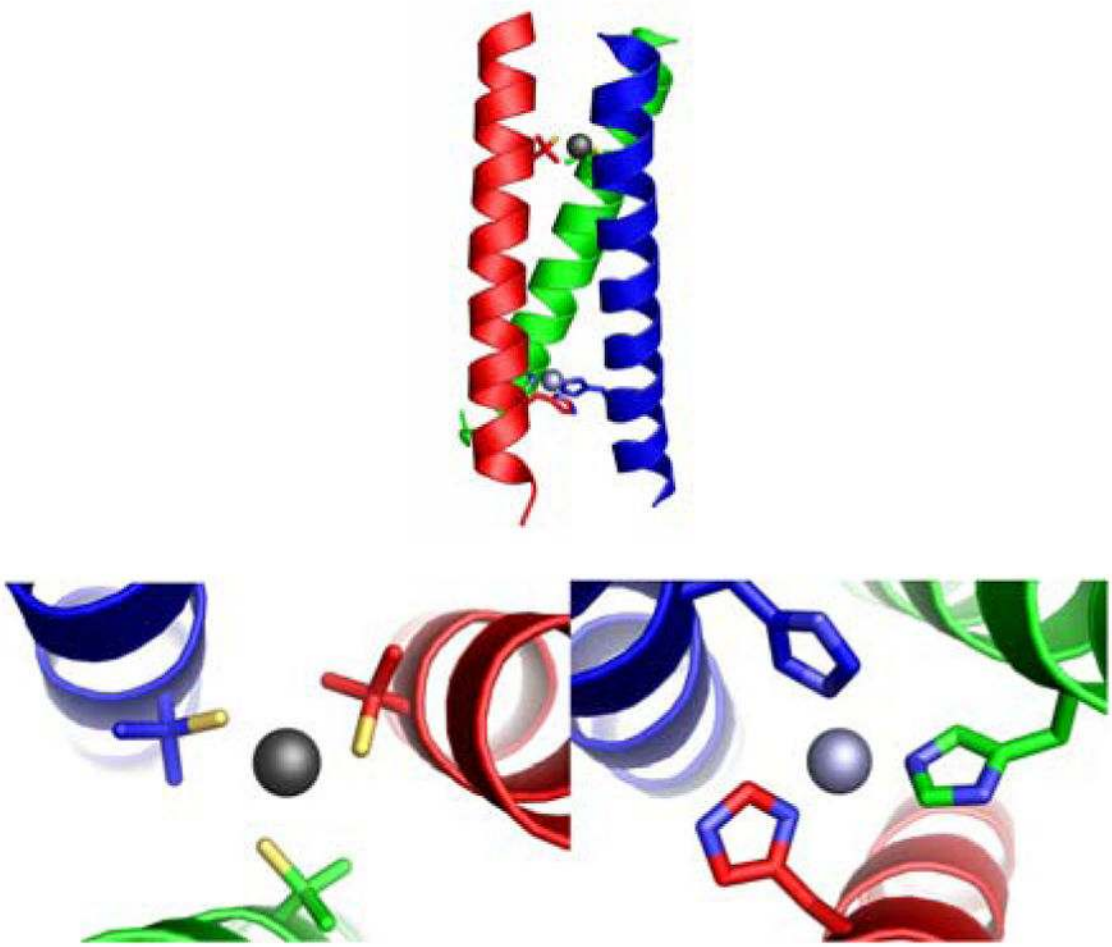

Figure 6.

(Top) X-ray crystal structure (PDB 3PBJ) of an artificial metalloenzyme $[Hg(II)]_S[Zn(II)(OH^-)]_N(TRIL9CL23H)_3$ with multiple metal-binding sites. (Bottom left) Binding of thiolates to Hg(II) provides stability to metalloenzyme. (Bottom right) The catalytic zinc site.

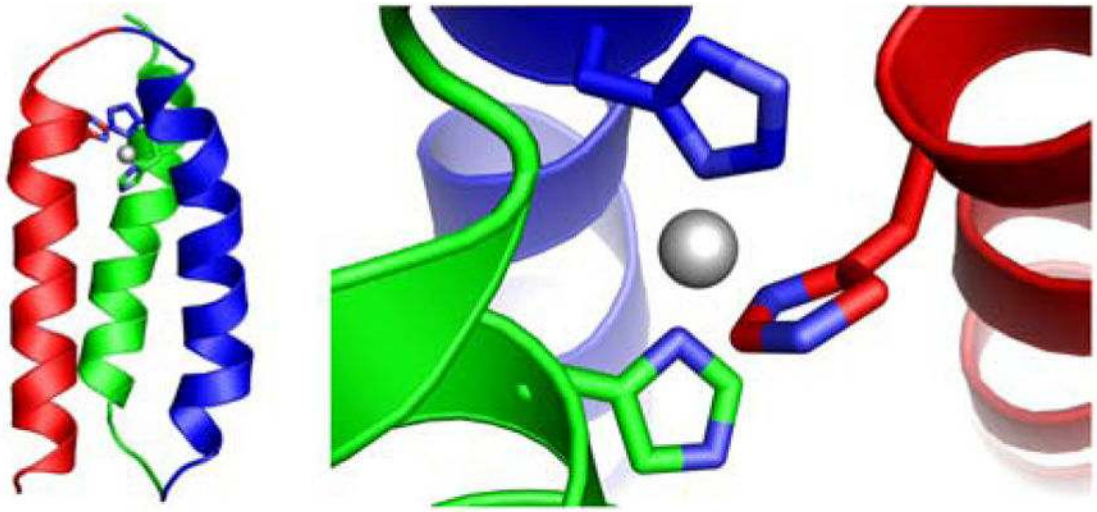

Figure 7.
Overall view (left) of the X-ray crystal structure of Zn(II)-binding protein (PDB 2A3D) α_3DH3 and its zinc-binding site (right).

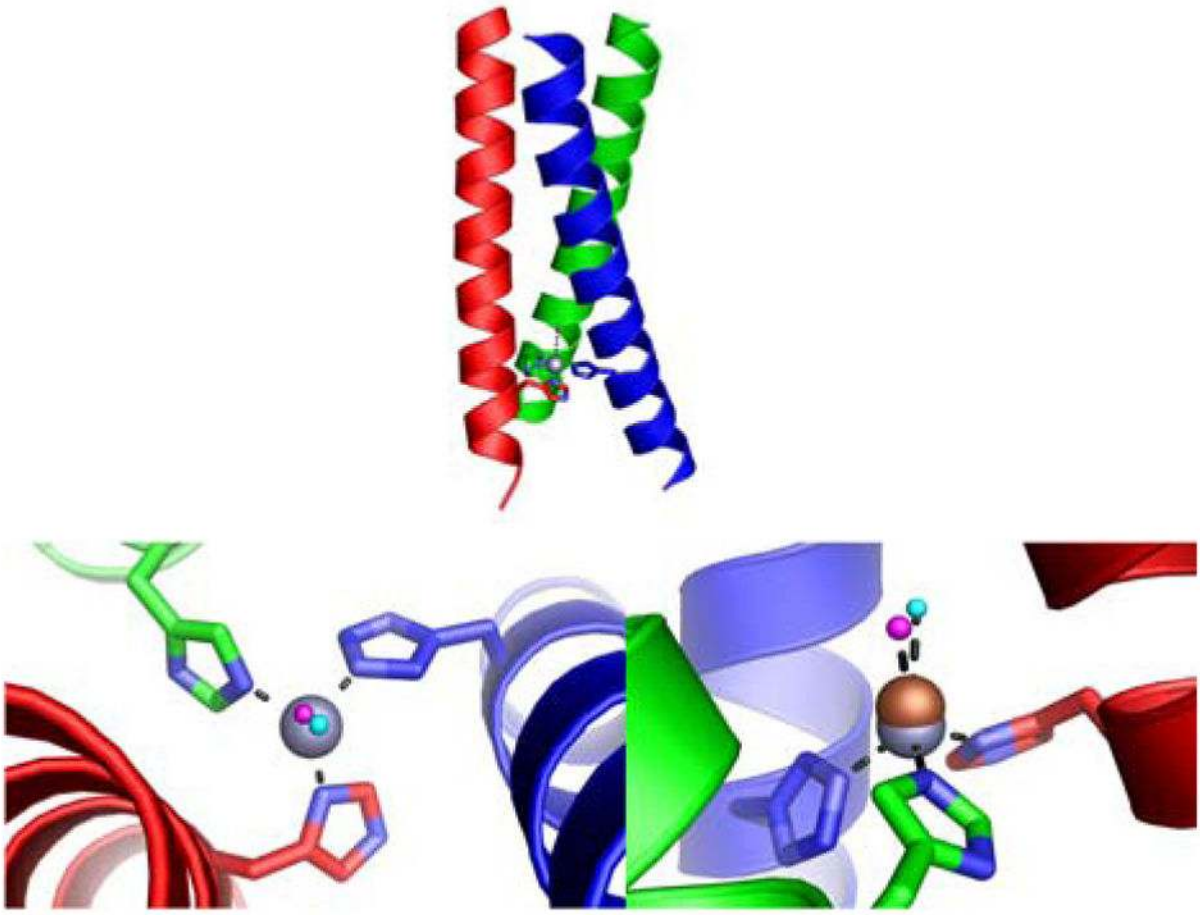

Figure 8.

(Top) The model of the peptide Cu(I/II)(TRIL23H)$_3$ based on a crystal structure of a related protein [Hg(II)]$_S$[Zn(II)(OH$^-$)]$_N$(TRIL9CL23H)$_3$ (PDB code 3PBJ). (Bottom left) Top-down perspective of the metal binding site in metallopeptide. (Bottom right) Comparison of the metal binding sites with Zn (gray) and Cu (brown). Water molecules from two different structures are shown as magenta and cyan spheres.

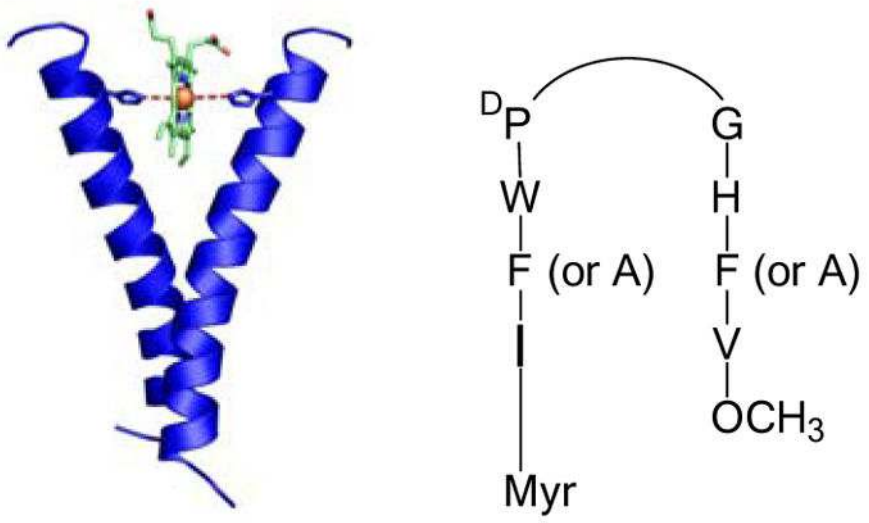

Figure 9.

(Left) Model of ME1 complex with hemin based on NMR structure of glycophorin A (PDB 1DWR). Flanking histidine residues on neighboring chains allows coordination of heme. (Right) Sequence of the rationally designed β-hairpin peptide with turn indication between ^{D}Pro-Gly segments.

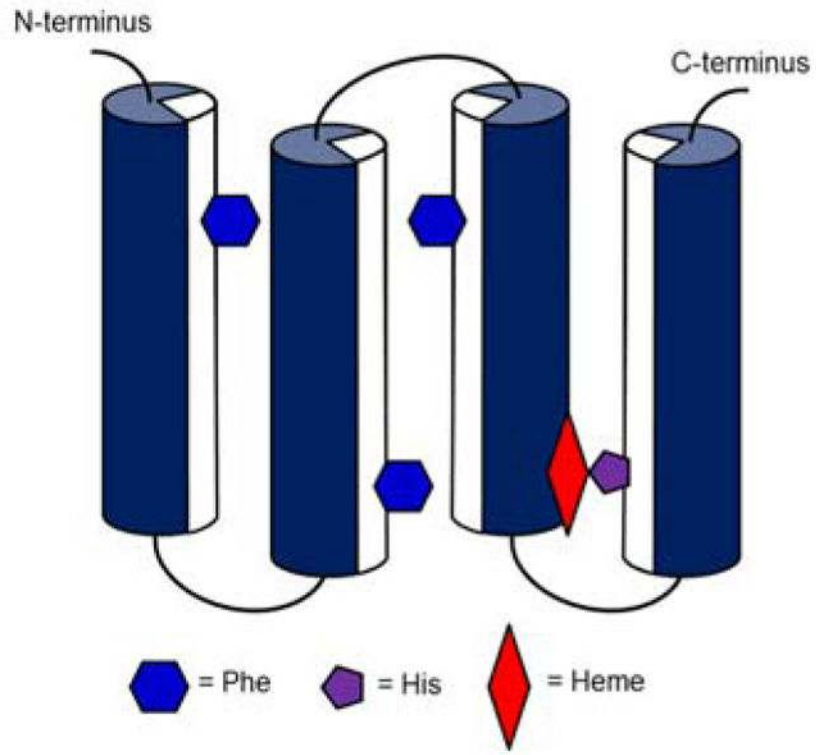

Figure 10.
Schematic representation of secondary elements of C45: His to Phe mutations help to stabilize the desired structure and direct heme binding to a histidine.

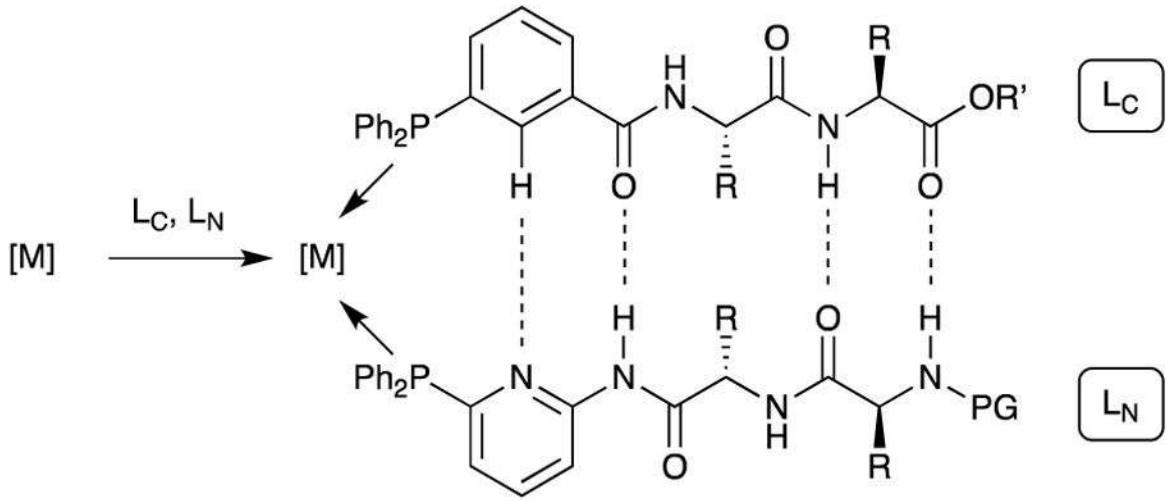

Figure 11.

Phosphane-functionalized peptides capable of noble metal binding and formation of β-sheets. Reproduced from ref. 73 with permission from Wiley-VCH Verlag GmbH & Co. KGaA, copyright 2008.

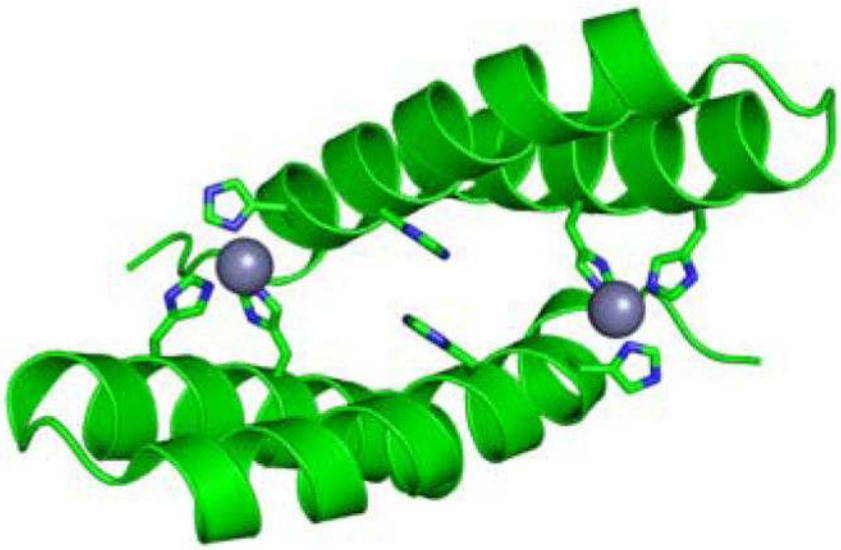

Figure 12.
A crystal structure of an artificial esterase MID1 (PDB code 3V1C).

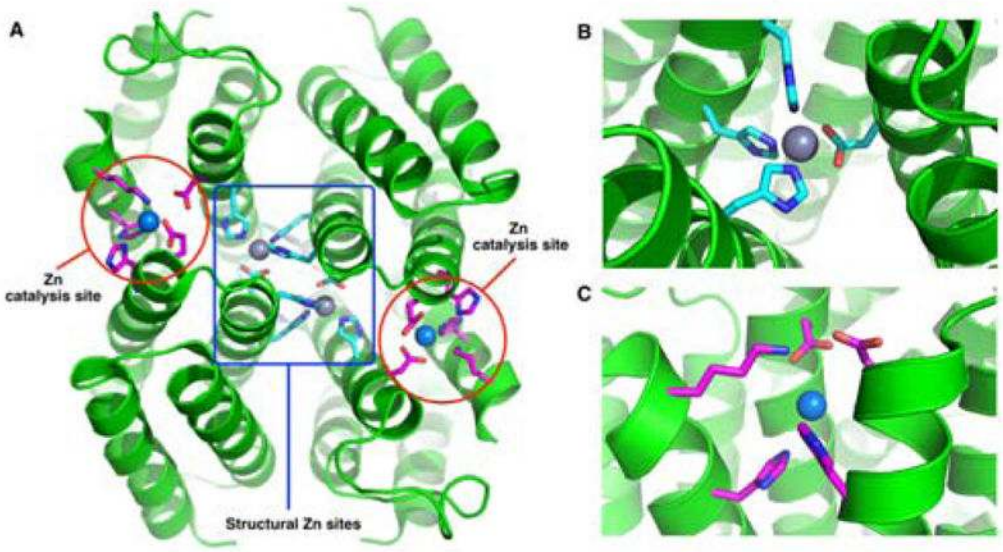

Figure 13.

(A) A crystal structure of the catalytically active artificial hydrolase, Zn_8:$AB3_4$ (PDB 3IQ6). Two types of sites – structural and catalytic- are indicated (only half of the bundle is shown for clarity). (B) Enhanced view of the structural zinc coordination sphere. (C) Enhanced view of the catalytic zinc coordination sphere.

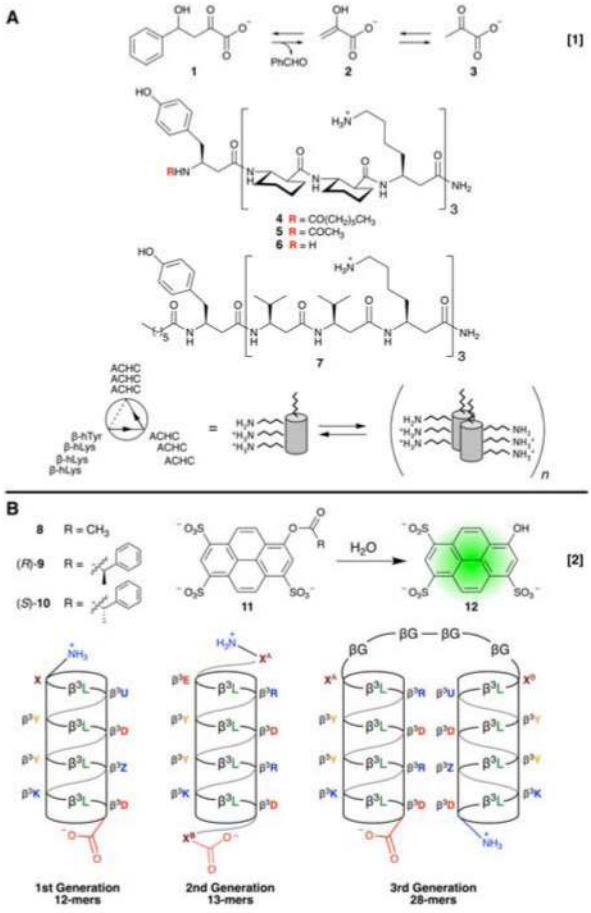

Figure 14.

(A) Retroaldol-catalyzed reaction of **1** by catalytic assemblies **4**–**6** derived from ACHC-scaffold or assembly **7**. A helical-wheel diagram of the β-peptide (left) and cartoon representation of the assembly (right) are shown. (B) Helical diagrams of β^3-peptide assemblies (1st, 2nd, and 3rd generations) tested in the hydrolysis of pyrene trisulfonate esters. Reproduced from ref. 84 and 86 with permission from Wiley-VCH Verlag GmbH & Co. KGaA (copyright 2008) and from the American Chemical Society, (copyright 2014).

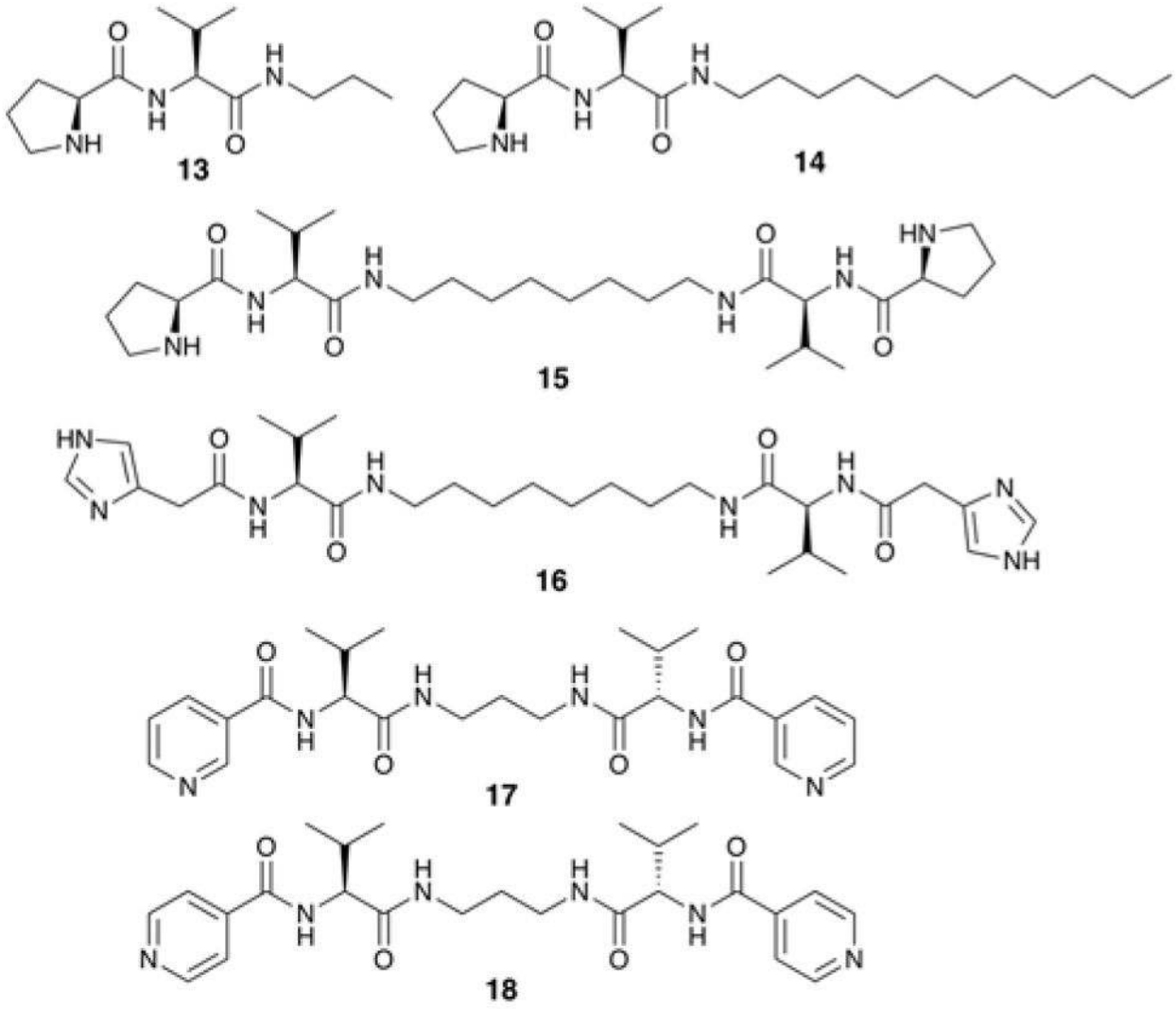

Figure 15.
Representative catalytic gelators developed by Escuder, Miravet and co-workers.

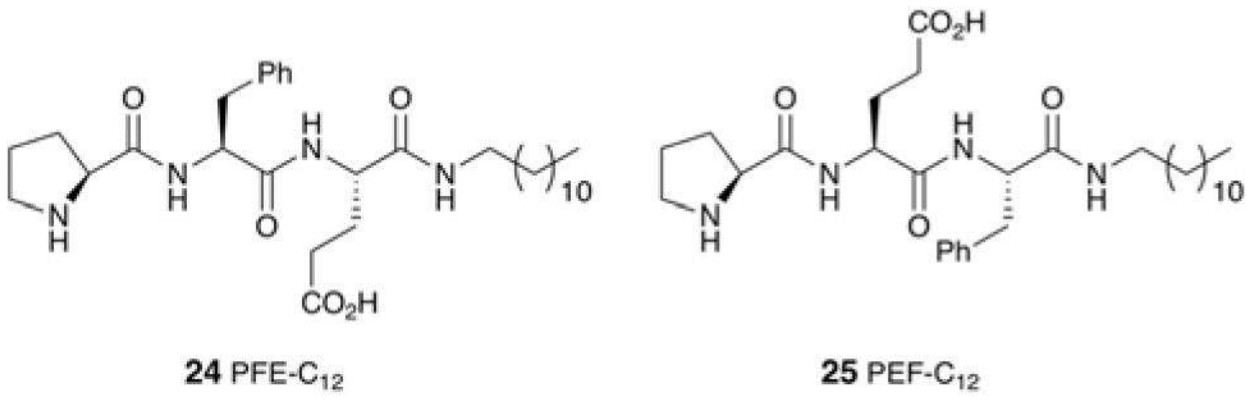

Figure 16.
Pro-Phe-Glu-based catalysts capable of aldol reaction catalysis.

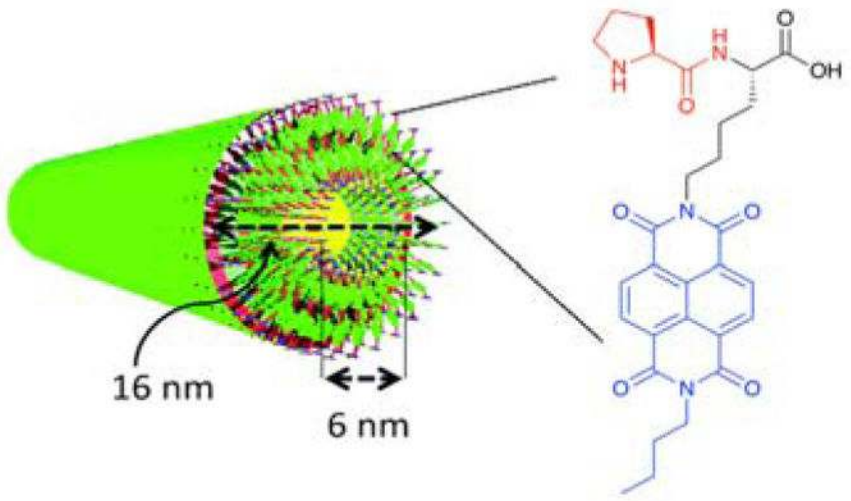

Figure 17.
A model for catalytic nanotubes formed by Pro-Lys-NDI. Adapted from ref. 110 with permission from the Royal Society of Chemistry, copyright 2015.

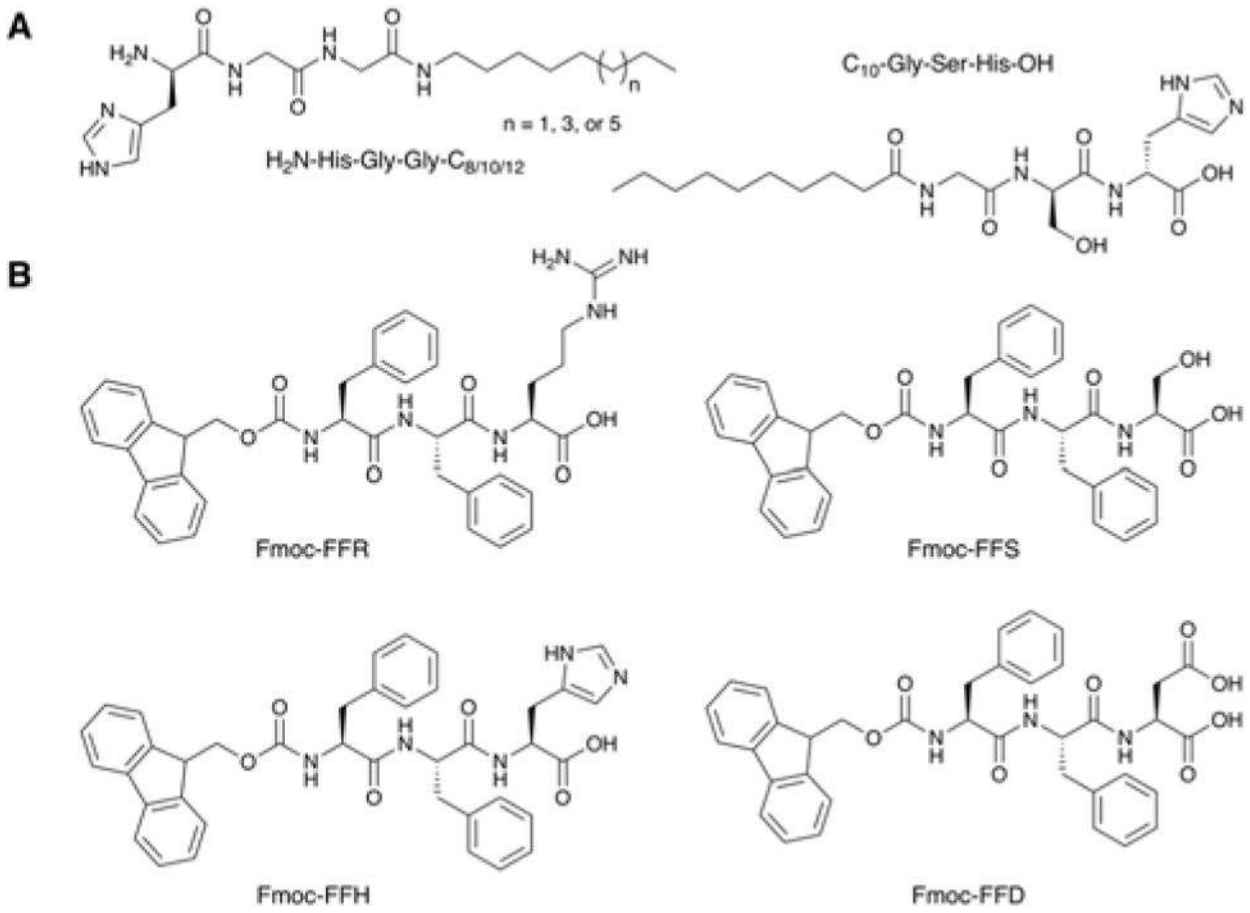

Figure 18.

Selected examples of C- and N-protected histidine-based tripeptides used to form self-assembled catalysts. (A) Tripeptides with C- and N-terminal lipophilic attachment and (B) Fmoc-protected tripeptides as a source of catalytic activity upon assembly.

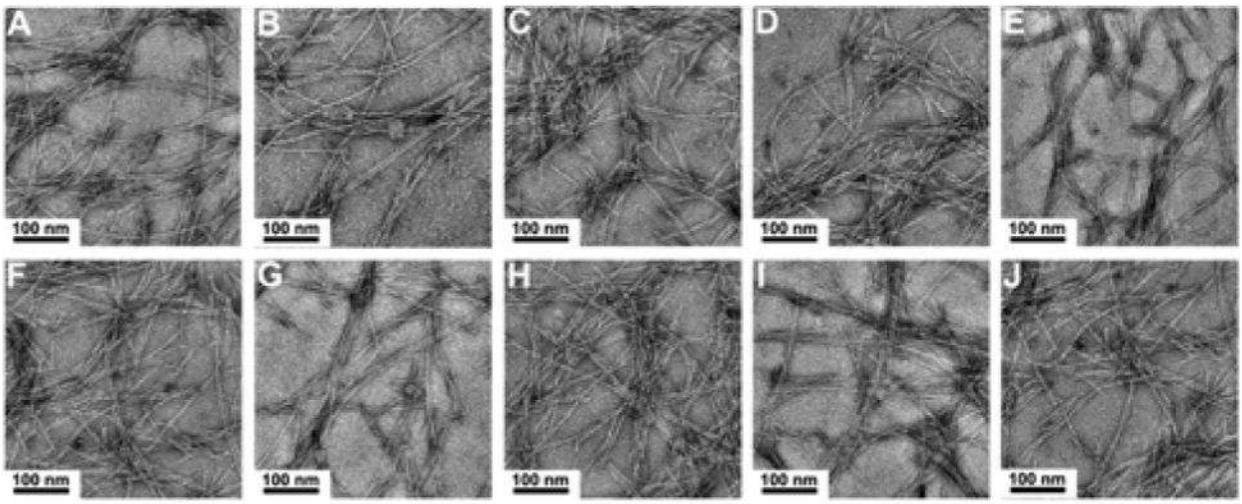

Figure 19.

TEM Images of the Q11 family peptides indicating the presence of distinct fibrillar network in all cases. (A) Q11G, (B) Q11H, (C) Q11R/H = 1:20, (D) Q11R/H = 1:15, (E) Q11R/H = 1:10, (F) Q11R/H = 1:2, (G) Q11R/H = 1:1, (H) Q11R/H = 2:1, (I) Q11R/H = 10:1, (J) Q11R. Reproduced from ref. 119 with permission from the American Chemical Society, copyright 2014.

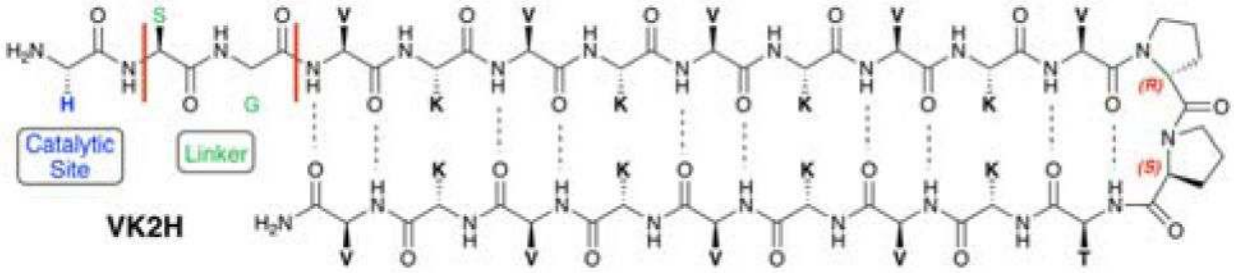

Figure 20.

Self-assembling peptide **VK2H** formed by attaching a catalytic His (blue) to **MAX1** with a Ser-Gly linker (green).

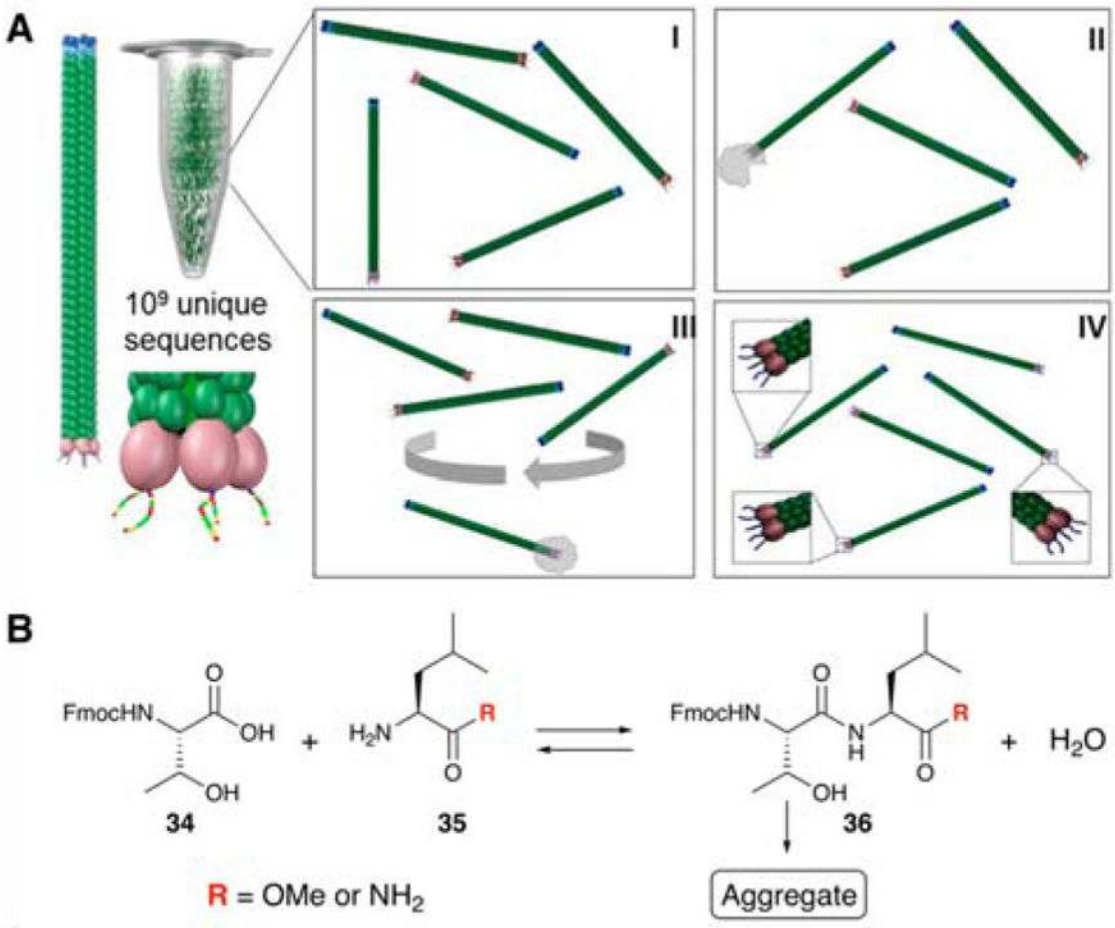

Figure 21.

Illustration of screening phage libraries for catalytic activity. (A) Four cycles of phage replication were necessary to generate an expansive library of sequences. (B) Dipeptides formed by condensation of Fmoc-Thr with leucine derivatives aggregate driving the equilibrium to the right. Reproduced from ref. 124 with permission from the American Chemical Society, copyright 2014.

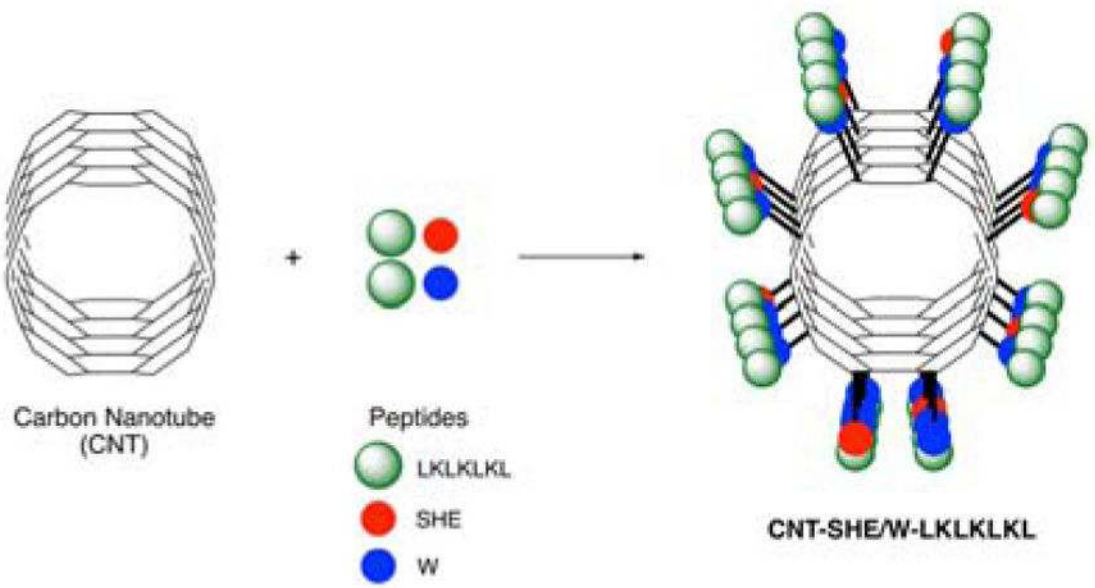

Figure 22.

A proposed arrangement of components in a hybrid nanomaterial based on self-assembly of CNT and peptides. The peptide-CNT assembly allows for a bilayer of peptides to assemble through covalent interaction first by a random-mixed assembly of SHE and W peptides. Reproduced from ref. 127 with permission from the Royal Society of Chemistry, copyright 2016.

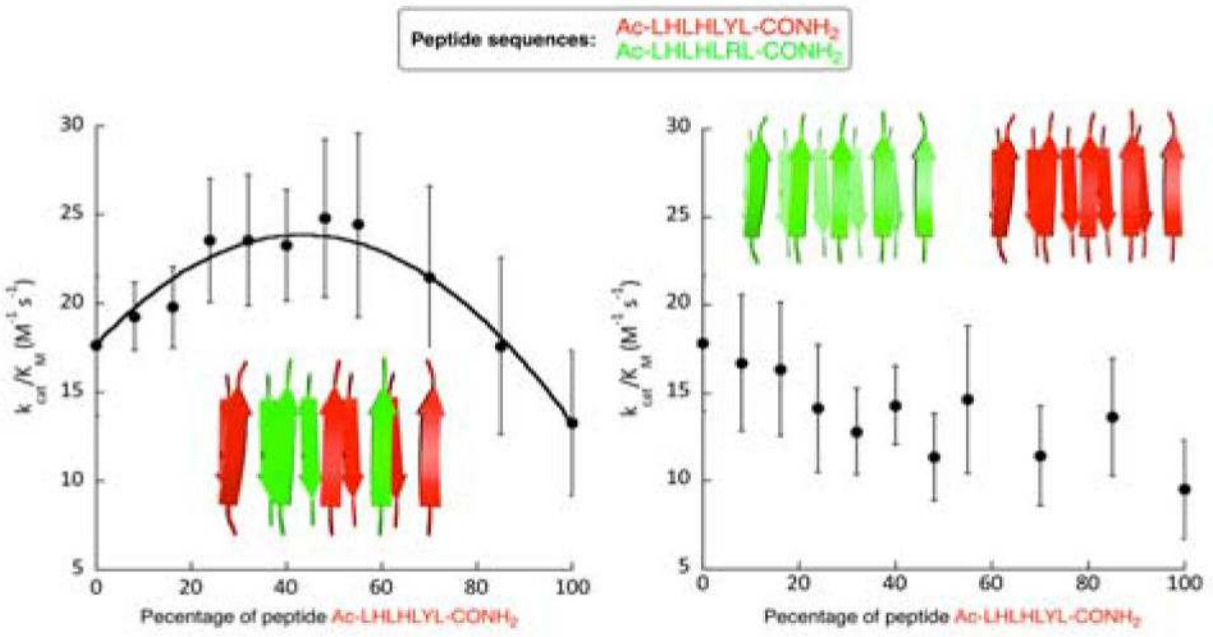

Figure 23.

Illustration of synergistic effect in catalytic amyloids. Fibrils formed from a mixture of peptides (left) show higher activity than homomeric peptide mixtures (right). Reproduced from ref. 133 with permission from Nature Publishing Group, copyright 2014.

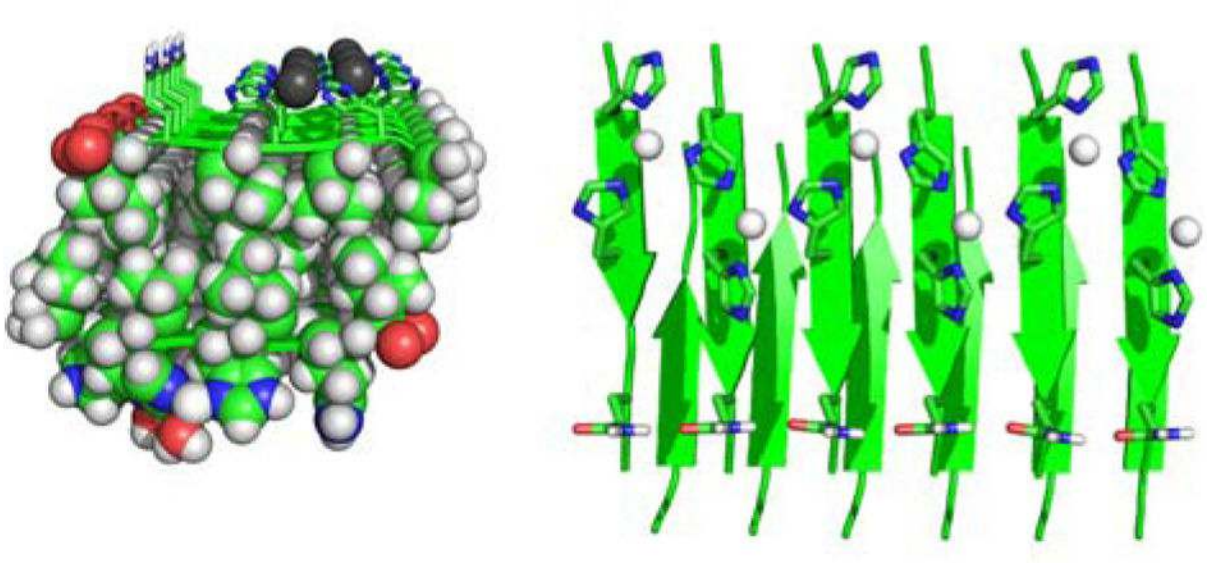

Figure 24.
The structure of catalytic amyloids deduced from ssNMR showing tight packing of the hydrophobic core (left) with characteristic zigzag pattern of zinc atoms (right), PDB code 5UGK. Reproduced from ref. 134 with permission from National Academy of Sciences, copyright 2017.

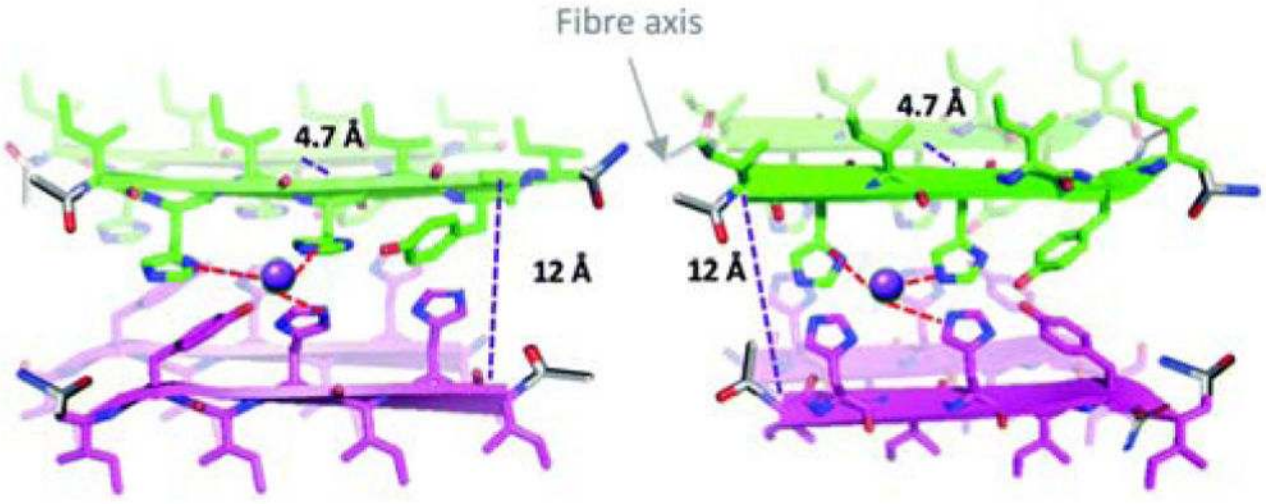

Figure 25.

Proposed structure based on X-RFD data for the peptide assemblies formed by Ac-IHIHIYI-$CONH_2$. Reproduced from ref. 138 with permission from the Royal Society of Chemistry, copyright 2017.

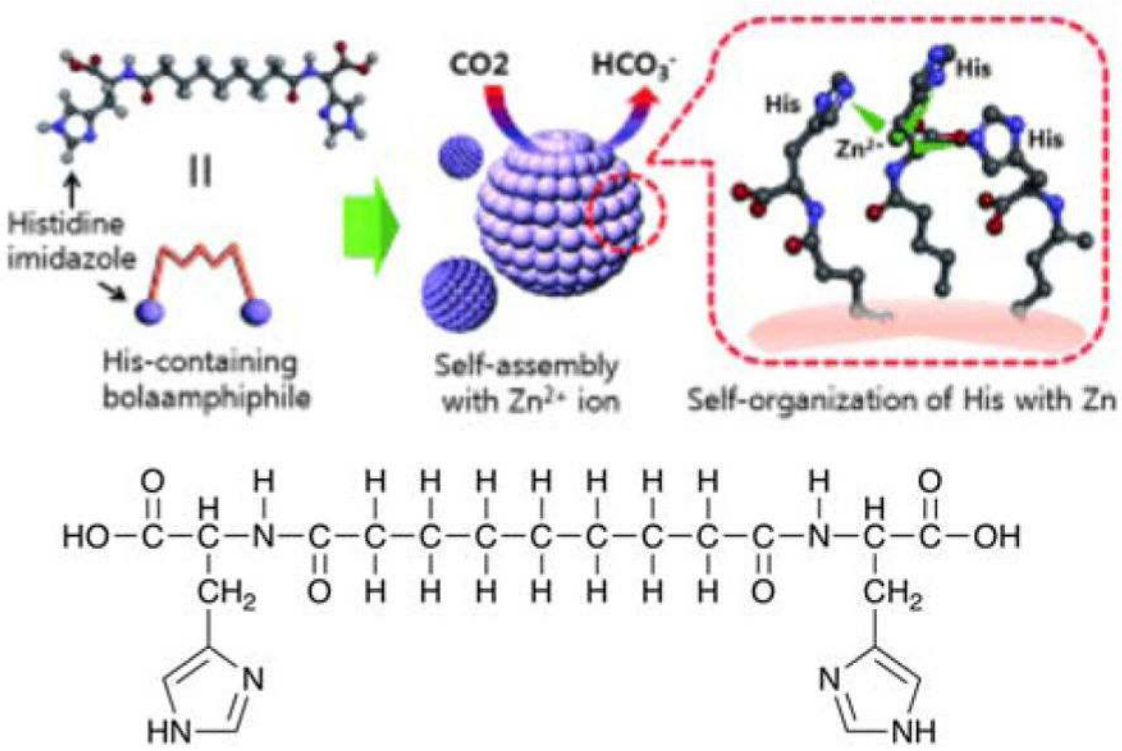

Figure 26.

Artistic rendition of bolaamphiphilic histidine-based peptides self-assembling into the blob-like structures capable of catalytic CO_2 hydration. Reproduced from ref. 142 with permission from Wiley-VCH Verlag GmbH & Co. KGaA, copyright 2014.

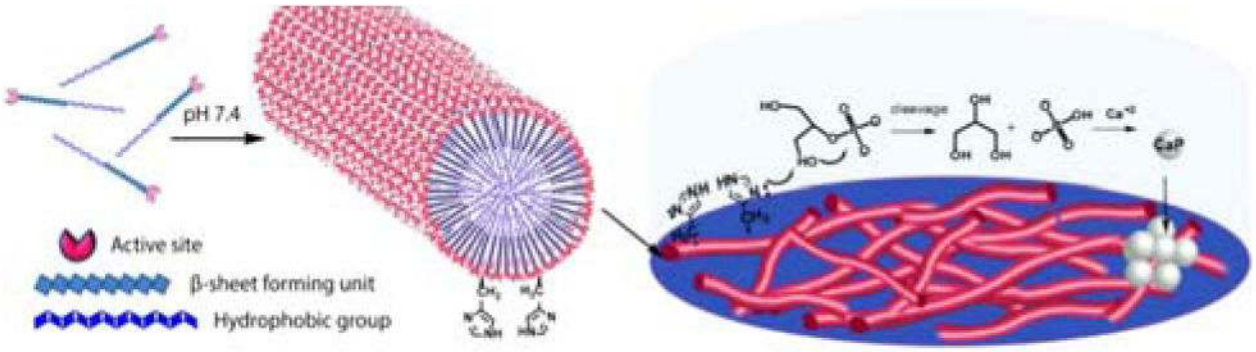

Figure 27.

A model for catalytic phosphatase-like peptide assembly with additional bone regeneration function. Reproduced from ref. 145 with permission from the American Chemical Society, copyright 2016.

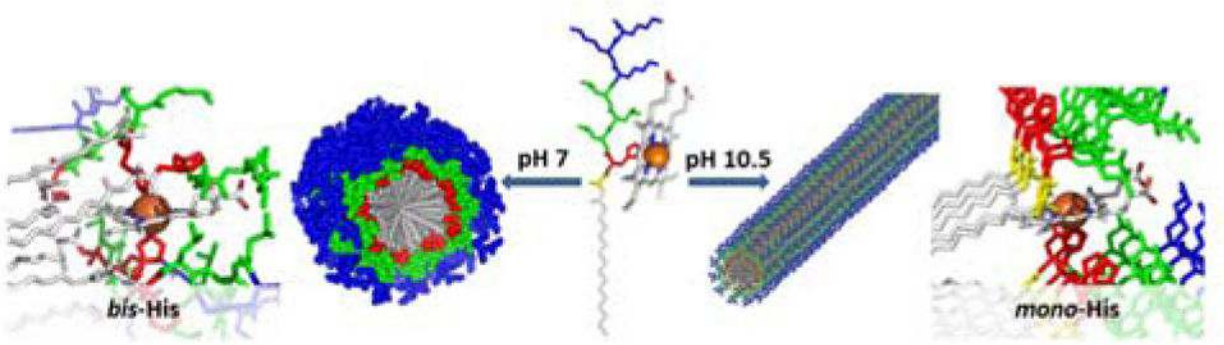

Figure 28.

Proposed model of heme-binding peptide amphiphile catalytic assemblies that are regulated by pH. Reproduced from ref. 146 with permission from the American Chemical Society, copyright 2017.

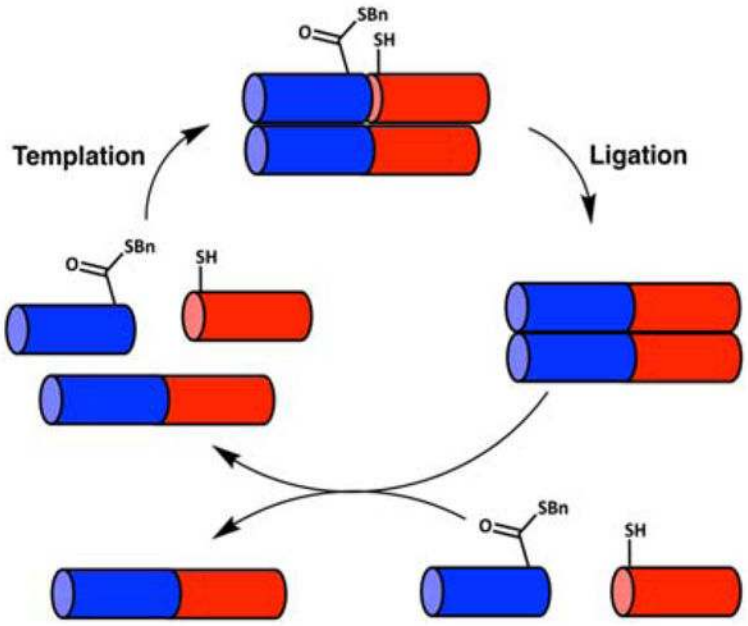

Figure 29.
Self-replicating system that promotes native chemical ligation in a hypercyclic fashion using an α-helical peptide template.

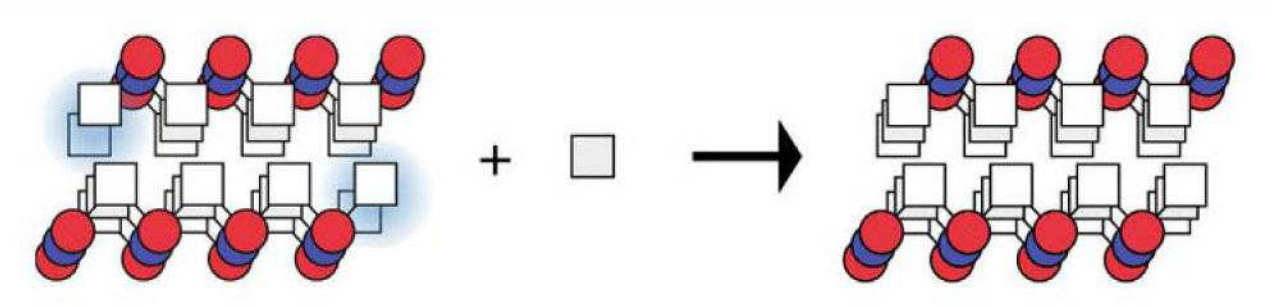

Figure 30.
Schematic representation of a template-assisted condensation of activated amino acid.
Reproduced from ref. 155 with permission from Nature Publishing Group, copyright 2018.

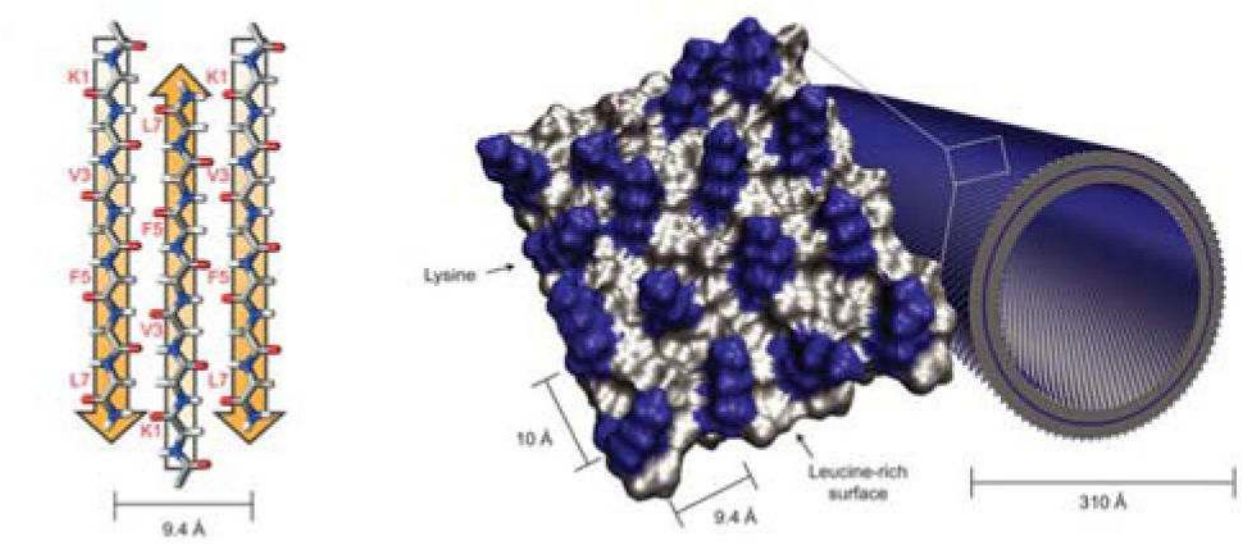

Figure 31.

Self-assembled structures formed by peptide K1. The model is based on computational studies and cryo EM data. Reproduced from ref. 156 with permission from Nature Publishing Group, copyright 2017.

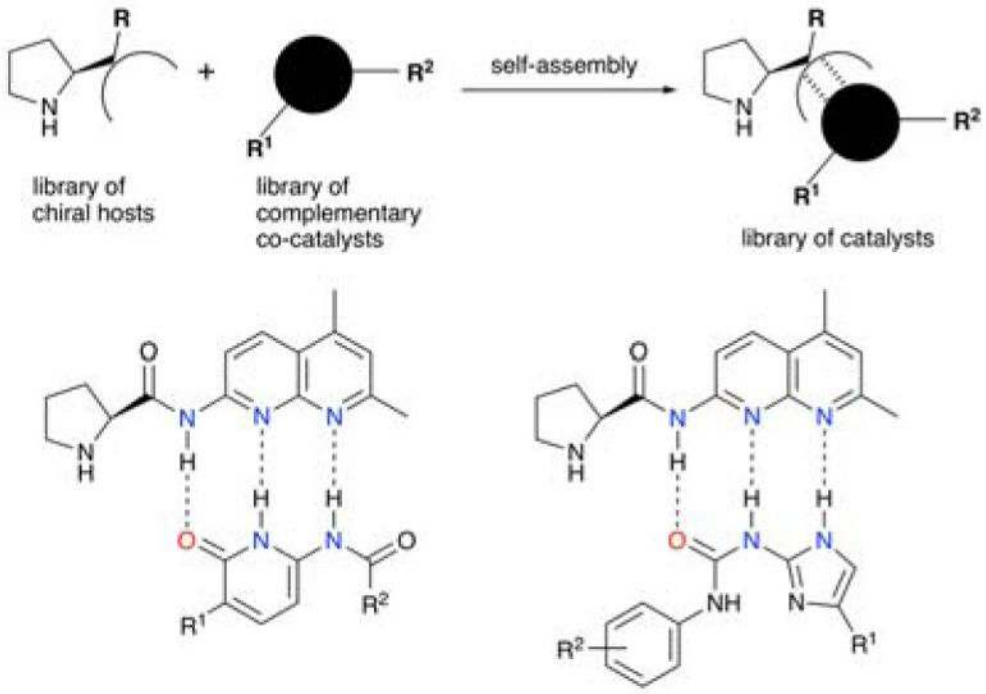

Scheme 1.

Self-assembly of Pro-Nap with co-catalysts. Reproduced from ref. 51 with permission from the Royal Society of Chemistry, copyright 2011.

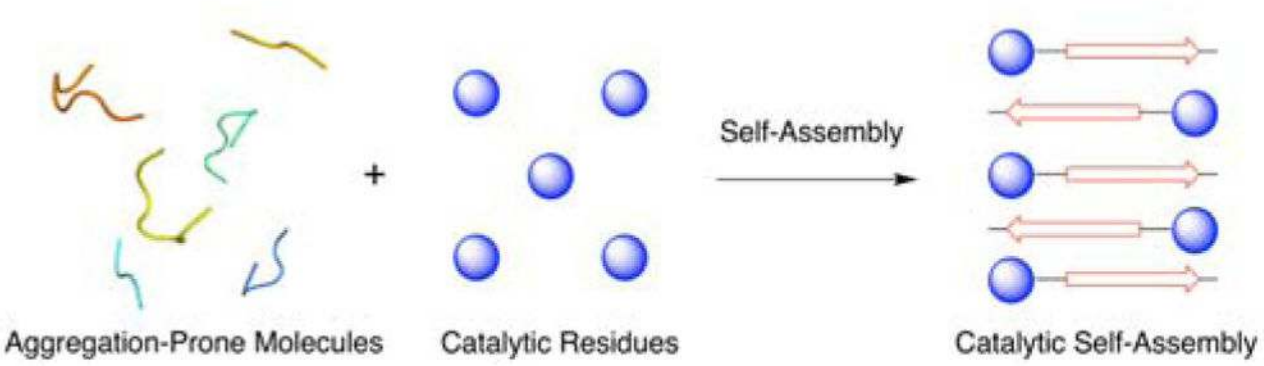

Scheme 2.
Overall approach to creating self-assembling peptide catalysts.

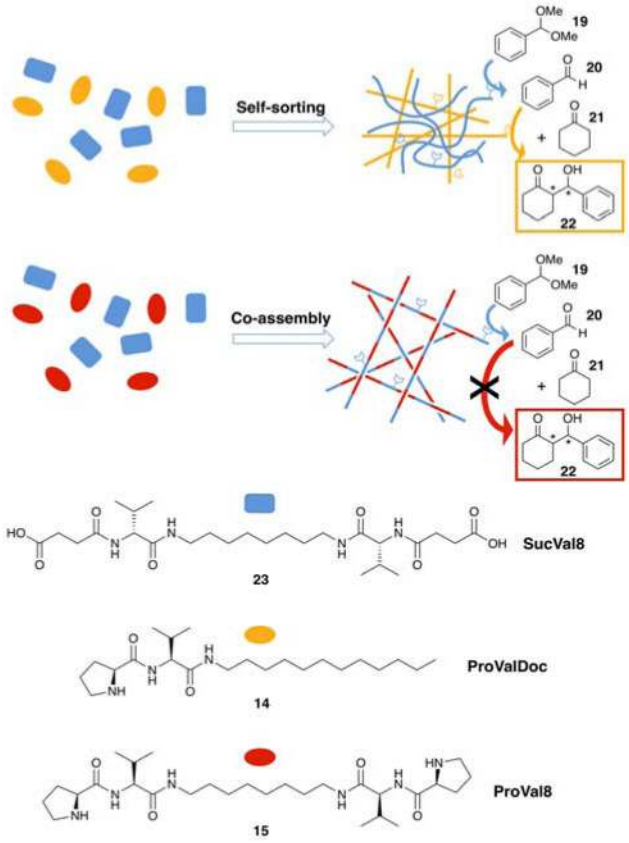

Scheme 3.

Self-sorting versus co-assembly in tandem deacetalization/aldol coupling reaction. Randomly assorted fibrils that "self-sort" facilitate conversion of the acetal to the aryl aldehyde and its subsequent aldol coupling with cyclohexanone. Co-assembled fibrils do not promote aldol coupling. Reproduced from ref. 105 with permission from the Royal Society of Chemistry, copyright 2016.

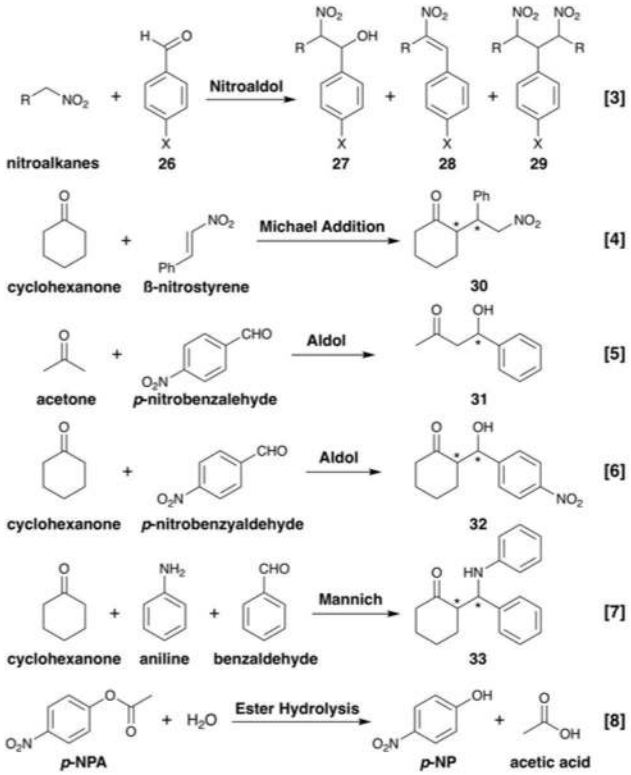

Scheme 4.

Various standard chemical transformations known to be catalyzed by self-assembled peptide catalysts.

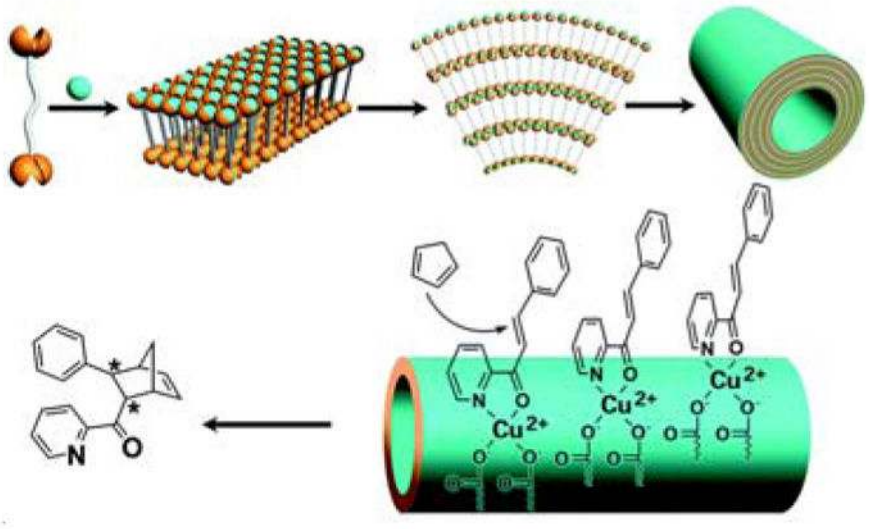

Scheme 5.

Formation of catalyst by self-assembly of monomers into multi-layered nanotubes (blue cylinders) in the presence of Cu(II) (blue spheres). Reproduced with permission from ref. 131. Reproduced from ref. 131 with permission from the American Chemical Society, copyright 2011.

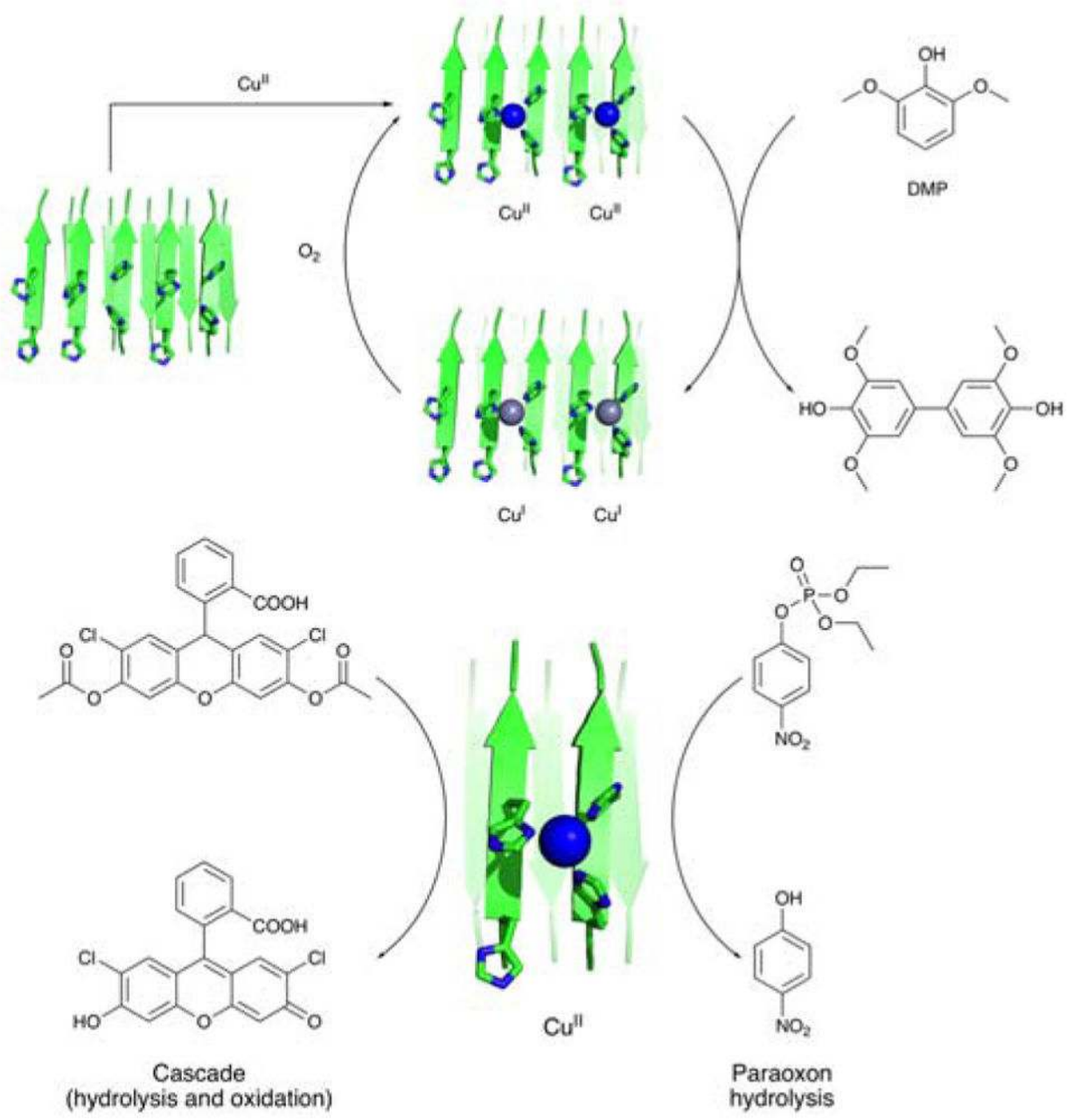

Scheme 6.

Representative model of copper-binding catalytic amyloids capable of catalyzing oxidative (top), hydrolytic (bottom right) and cascade (bottom left) reactions. Reproduced from ref. 136 and ref. 140 with permission from the American Chemical Society (copyright 2017) and from Wiley-VCH Verlag GmbH & Co. KGaA (copyright 2016).

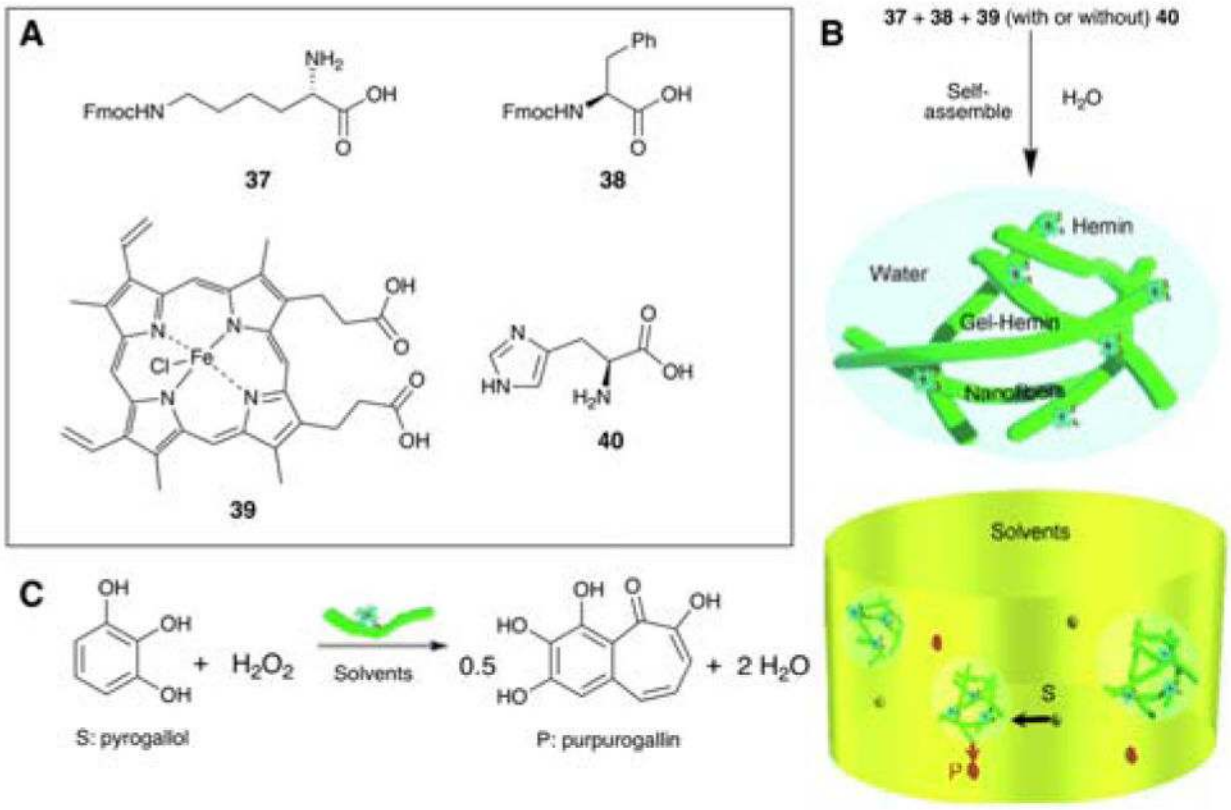

Scheme 7.

Building blocks (A) self-assemble into catalytic network (B). Oxidation reaction catalysed by the resulting assembly (C). Reproduced from ref. 147 with permission from Wiley-VCH Verlag GmbH & Co. KGaA, copyright 2007.

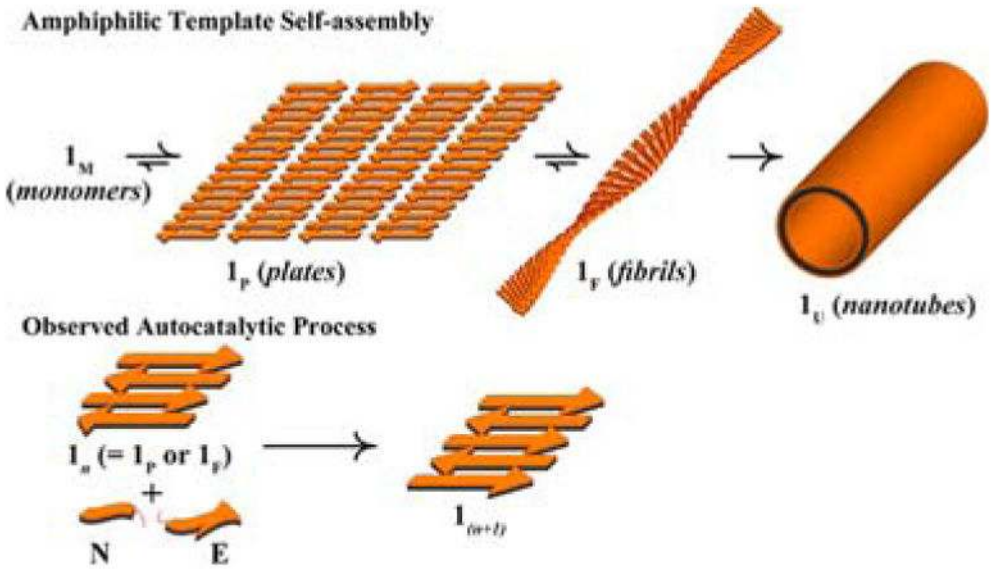

Scheme 8.

Peptide monomers self-assemble into β-sheets followed by fibrils and, finally, nanotubes. The autocatalytic process demonstrates elongation of β-sheets. Reproduced from ref. 153 with permission from the American Chemical Society, copyright 2012.